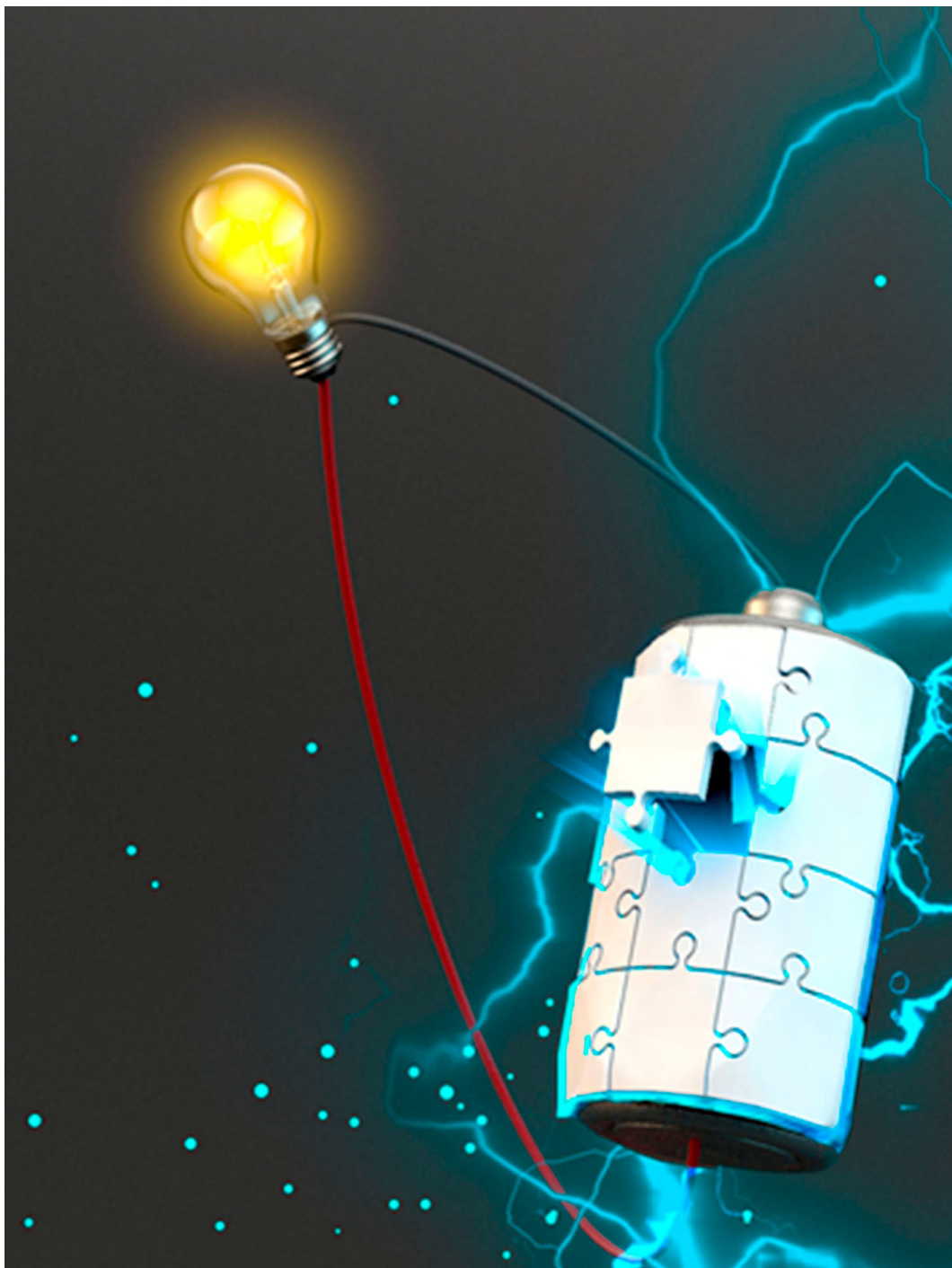


Recent Progress in Binder-Free Electrodes Synthesis for Electrochemical Energy Storage Application

Kaixiang Shen^{+, [a, b]} Shengli Zhai^{+, [a, b]} Shaofeng Wang,^[a, b] Qiang Ru,^[a, b] Xianhua Hou,^[a, b] Kwan San Hui,^[c] Kwun Nam Hui,^{*[d]} and Fuming Chen^{*[a, b]}



Fabrication of binder-free electrodes is an effective way to increase the performance of electrochemical energy storage (EES) devices, such as rechargeable batteries and supercapacitors. In traditional electrodes, the binder is usually electrochemically inert and has weak interactions and interfaces between binder and the active material, which increase "dead mass" and directly affect the performance of energy storage system. The binder-free electrode can provide well-designed electrode material structure enables well connection between active materials themselves and current collectors. In addition, without insulating binder, electron and electrolyte ions can transfer more efficiently within the electrode materials. Here, we reviewed research efforts in using various techniques involving

chemical, physical and electrical methods to fabricate binder-free electrodes. For every technique, we first briefly describe their principle and involved factors that influence the performance of as-fabricated binder-free electrodes and summarize advantages and disadvantages. Next, we reviewed several works which have used this technique to fabricate binder-free electrodes. Further, the effect of well-crafted structure design on the properties of energy storage performances including rate capability, and cycle stability was highlighted. Last, we offer our perspectives on the challenges and potential future research directions in this area. We hope this review can stimulate more research to design and synthesize the binder-free materials for EES devices.

1. Introduction

Due to the gradual depletion of fossil fuels and the concern on environmental protection, the demand for sustainable power sources such as solar energy, tidal energy and wind energy is increasing.^[1–2] While these renewable energies have been widely used in modern industry, their season- and whether-dependent nature make them fail in continuous energy supply. Electrochemical energy storage (EES) devices which are free of the above issues emerges as an important technology to integrate renewable resources into electric grid by efficiently storing energy from these intermittent power sources.

As the two most important members of EES family, supercapacitors (SCs) and secondary batteries have been widely and systematically studied. SCs store energy through electrical double layer capacitance by reversible electrolyte ion adsorption on the surface of electrode materials and pseudocapacitance through surface redox reactions. In general, SCs have the advantage of fast charge/discharge rate, high power density

and long life span.^[3–4] Secondary batteries such as lithium/sodium/potassium ion batteries (denoted as LIBs/NIBs/PIBs) store energy via various faradic reactions in the bulky electrode materials accompanied by a phase transformation. Therefore, secondary batteries could provide high energy density with steady discharge platform.^[5–6] For SCs and secondary batteries, dedicatedly designed electrodes are a crucial component to enable high electrochemical energy storage performance.^[7] In general, most electrodes are fabricated by coating slurries of active materials, conductive additives (e.g., acetylene black) and binders on a conductive substrate (e.g., copper, aluminum, stainless-steel, conductive carbon). However, the electrode fabrication process includes multiple steps which involve various components and parameters (mass loading of active materials, ratio of different components, etc.). The correlation of these parameters with their effect on electrochemical performance is not yet clear. In addition, polymer binders such as polyvinylidene fluoride (PVDF), carboxymethylcellulose sodium (CMC) are generally inactive and may insulate electrode materials and conductive additives. It will result in the "dead mass",^[8] and significantly deteriorate capacity and increases manufacturing costs.^[9] Moreover, the binder-free electrodes avoid the utilization of binder and even current collectors in certain scenarios. Therefore, binder-free strategy is expected to improve the volumetric performance of electrochemical energy storage devices by reducing overall size. At the same time, the absence of binder and the unity of active materials and current collectors facilitate the utilization rate of active materials which further improve the volumetric performance by enhancing electrochemical performance. Therefore, it is still challenging to fabricate high-performance electrode via the slurry coating strategy. In this context, binder-free electrodes are particularly attractive recently because of the following advantages. 1) In binder-free electrodes, the active material and conductive substrates are well contacted, thus fast electron transport pathway can be provided and yield sufficient mass loading of active materials for high energy density.^[10] 2) Without the insulating binder, the electrolyte ions could efficiently access active materials while electrons can fast transfer within electrode.^[11] 3) Sufficient space can be offered via rich structural voids between adjacent nanostructures to withstand the large

[a] K. Shen,[†] Dr. S. Zhai,[†] Dr. S. Wang, Prof. Dr. Q. Ru, Prof. Dr. X. Hou, Prof. Dr. F. Chen
Guangdong Provincial Key Laboratory of Quantum Engineering and Quantum Materials
Guangdong Provincial Engineering Technology Research Center of Efficient Green Energy and Environmental Protection Materials
School of Physics and Telecommunication Engineering
South China Normal University
Guangzhou, 510006, China
E-mail: fmchen@m.scnu.edu.cn

[b] K. Shen,[†] Dr. S. Zhai,[†] Dr. S. Wang, Prof. Dr. Q. Ru, Prof. Dr. X. Hou, Prof. Dr. F. Chen
Guangdong-Hong Kong Joint Laboratory of Quantum Matter
Frontier Research Institute for Physics
South China Normal University
Guangzhou 510006, China

[c] Dr. K. San Hui
Engineering, Faculty of Science
University of East Anglia
Norwich, UK

[d] Prof. Dr. K. Nam Hui
Joint Key Laboratory of the Ministry of Education
Institute of Applied Physics and Materials Engineering
University of Macau
Avenida da Universidade, Taipa, Macau, PR China
E-mail: bizhui@um.ac.mo

[†] These authors contributed equally to this work

volume changes of the active material during charging and discharging.^[10] Thus, the binder-free electrodes have great potential for fabrication of high-performance energy storage devices.^[12] The studies on binder-free electrodes have triggered great research interest in exploration of corresponding synthesis strategy.^[3,13–14] Hence, it is essential to review the fabrication methods which are commonly employed in the recently reported binder-free electrodes.

In this review, we summarize several approaches to synthesize binder-free electrodes which have great potential for scalable production and being used in practical EES devices, including chemical vapor deposition (CVD), vacuum filtration, hydrothermal/solvothermal method, aerogel production, 3D-print, electrospinning, electrophoretic and electrochemical deposition (see Figure 1). Meanwhile, the electrochemical performances for the EES devices are also highlighted. Beyond that, we have also critically examined the current challenges and provided our perspectives on future research goals and

directions to improve the performance of binder-free electrodes from fabrication method perspective.

2. Synthesis of Binder-Free Electrodes and their Electrochemical Energy Storage Applications

2.1. CVD Synthesis

Chemical vapor deposition (CVD) is a method of decomposing high vapor pressure gas to form a dense and stable structure for coating technology, thin-film production and surface treatment or improvement.^[15] This technique has been widely applied in fabrication of electrode materials in electrochemical energy storage field.^[16–18] As illustrated in Figure 2a, in a typical CVD process, the heated substrate is exposed in one or more volatile precursor molecules (gas, liquid, and solid) which decompose and/or react to produce almost any metallic or



Kaixiang Shen is a PhD candidate in School of Physics and Telecommunication Engineering, South China Normal University (SCNU) under the supervision of Prof. Fuming Chen. His research interests are synthesis of advanced materials for Li-ion batteries and electrocatalytic desalination.



Shengli Zhai obtained his Ph.D. degree from Nanyang Technological University, Singapore. His research interests mainly focus on carbon nanomaterials and their application in batteries and supercapacitors.



Shaofeng Wang is an Lecturer at South China Normal University. He got his Ph.D. in Nanjing University of Technology. He researches focuses on nanostructured electrode materials for advanced Li-ion, Li-S batteries, and industrialization of Si-based anode materials for Li-ion batteries.



Qiang Ru is an Associate Professor in South China Normal University, Guangzhou, China. He received his Ph.D. degree in Materials Science from Guangdong University of Technology in 2006. During 2014–2015, he also conducted the research at the University of Houston as a visiting scholar. His research interest focuses on nanomaterials and devices for energy storage including lithium/sodium/potassium ion batteries, aqueous batteries, and theoretical calculations based on Density Functional Theory.



Xianhua Hou is a Professor of School of Physics and Telecommunication Engineering at South China Normal University. He received his Ph.D. in Physical Chemistry from South China Normal University in 2009. His research focuses on nanostructured energy materials and electrochemical energy storage devices, such as Li-ion, Li-S, Na-ion batteries and industrialization of Si-based anode materials for Li-ion batteries.



Kwan San Hui is a Reader in Mechanical Engineering of School of Engineering, University of East Anglia. He obtained his Ph.D. degree in mechanical engineering at the Hong Kong University of Science and Technology (2008). His research focuses on advanced materials for energy storage, conversion and electrocatalysis.



Kwun Nam Hui is an Associate Professor of Institute of Applied Physics and Materials Engineering, University of Macau. He obtained his Ph.D. degree from The University of Hong Kong (2009). His research focuses on electrochemical energy storage and conversion (Na-ion batteries, flexible supercapacitors, fuel cell).



Fuming Chen is a Professor of School of Physics and Telecommunication Engineering, South China Normal University (SCNU). He received his Ph.D. from the Nanyang Technological University at Singapore in 2010. His current research interests are focused on advanced functional materials for electrochemical energy storage and desalination.

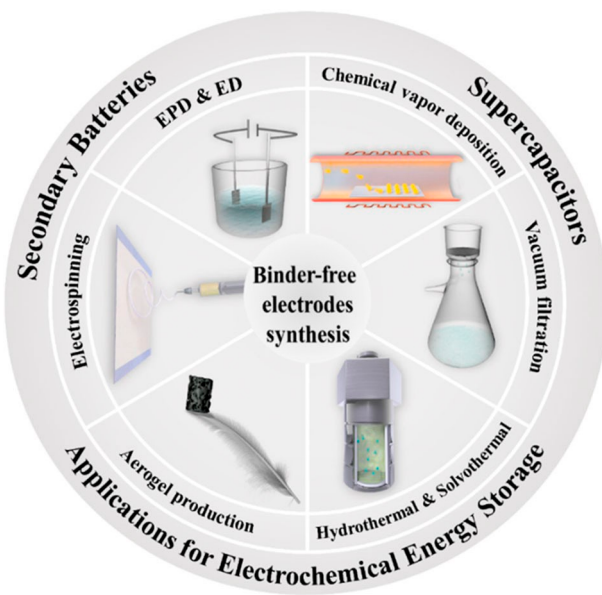


Figure 1. Illustration for synthesis strategies of binder-free electrodes in electrochemical energy storage.

ceramic thin film.^[19–21] Experimental factors including temperature, reaction chamber pressure, gas flow rate and distance between the source and substrate are able to influence the layers, size, morphology, dopants and defects of coating layers.^[22] For example, low nucleation density can be obtained via a high growth temperature with lower reactants flow rate (or partial pressure).^[23] The manipulation of these experimental factors make it possible to precisely control uniformity of coating layers and the thickness on nano- or even angstrom-level.^[24,25]

In order to obtain sample with uniform thickness distribution, Ren et al. employed the CVD method to grow amorphous FePO₄ (FP) on commercial carbon nanotubes (CNTs) fibers,

yielding freestanding binder-free CNT@FP electrodes (see Figure 2b).^[26] Without insulting binder particles, the connection between the active materials and CNTs can be maximized. The thickness of CVD-grown film can be controlled by varying the deposition time. The thickness of FePO₄ layer is around 20 nm under a 40-min deposition (Figure 2c). In addition, as-prepared CNT@FP fabric exhibited excellent mechanical properties including a tensile strength of 40–60 MPa and a maximum tensile strain of 25 %, which had great potential for applications in flexible batteries. Owing to multiple defects, the amorphous FP offered important kinetic advantages for fast Na⁺ transport. As cathode of a Na-ion half-cell, it could deliver a high capacity of ~150 mAh g⁻¹ as well as excellent rate capability and cycling stability (Figure 2e–g).

To enhance electron transport outside active materials and inhibit side reactions, Yao et al.^[27] reported a one-step CVD method to assemble binder-free metal sulfides with N-doped carbon (NC) coating. The thiourea precursor was placed in the first reaction area as the nonmetal source and cleaned nickel foam substrate was placed in the second reaction area. The obtained NC coated single crystalline Ni₃S₂ nanowires exhibited taper structures along the axial direction, with a diameter of 40–60 nm. The coated NC not only improved the electronic conductivity but also limited dissolution of polysulfide during cycling. Also, this nanowire structures can buffer the large volume expansion and prevent pulverization of active materials during charging/discharging. Thereby, the assembled Li-ion half-cell achieved a large capacity of 385 mAh g⁻¹ at 2 A g⁻¹ and excellent cycling stability of 91 % after 100 cycles at 1 A g⁻¹.

Besides conventional CVD techniques, the plasma-enhanced chemical vapor deposition (PECVD) is another well-established technique for deposition of a wide variety of films. PECVD provides a rich chemical environment including free radicals, photons, energetic electrons excited molecules and active ions.^[24,28] In general, PECVD has many advantages over conventional CVD techniques including low cost, low deposi-

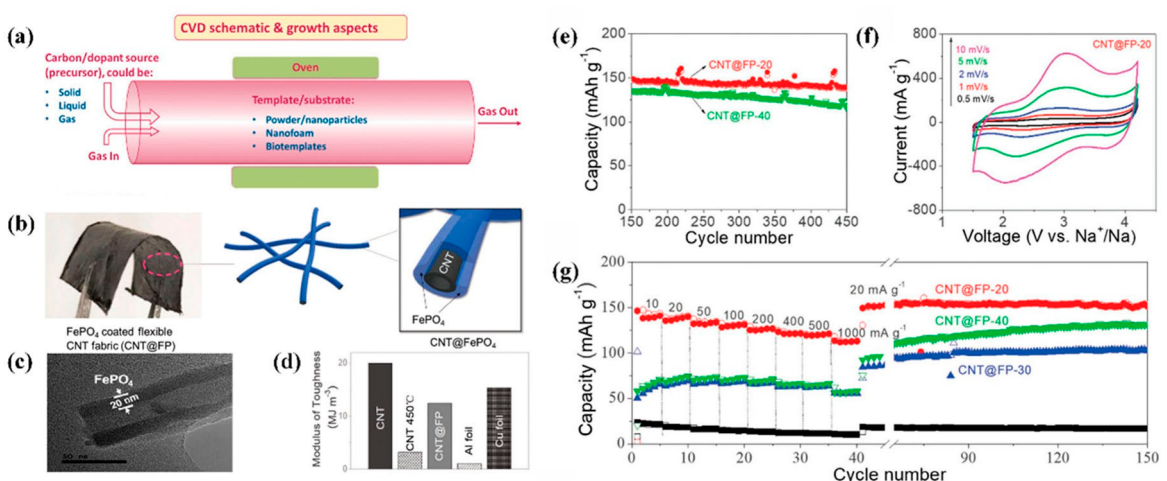


Figure 2. a) Schematic illustration of a CVD reactor. Reproduced with permission. Reproduced from Ref. [21] with permission. Copyright 2019, The Authors. b) Scheme of the fabrication of CNT@FP electrode, c) TEM image of the CNT@FP composite fiber, d) moduli of toughness of CNT, CNT@FP, and other materials, e) cycling performances of CNT@FP-electrodes, f) cyclic voltammetry profile of the CNT@FP electrode at different scan rates, and g) specific gravimetric performance of CNT@FP electrodes at different rates cycled between 1.5 and 4.0 V. Reproduced from Ref. [26] with permission. Copyright 2018, Wiley-VCH.

tion temperature, short deposition time, fast growth rate, high controllability and high purity of resulting products.^[29–30] Therefore, PEDVD becomes a popular method to synthesize graphene including vertically oriented graphene (VG).^[31] The typical morphology of VG with a three-dimensional architecture exhibits both large surface area and excellent electrical conductivity.^[32] Ouyang et al.^[33] prepared three-dimensional vertical graphene (3DVG) on porous nickel foams by a PECVD system with radio frequency plasmas, followed by removing the nickel foams through an etchant solution. Then MoS₂ nanosheets were grown on 3DVG foams via a hydrothermal approach. The morphology of resulting 3DVG and MoS₂@3DVG foam is shown in Figure 3a–b and d–e, respectively. Figure 3c illustrates the growth model of VG. In brief, the substrate surface is negatively charged relative to the bulk plasma, which creates an electric field and the Debye sheath on the substrate surface. Then hydrogen plasma dissociated the hydrocarbon of oil precursor vapors to produce carbon radicals and form several nucleation sites. When the carbon precursor with high surface mobility combined with the polarized local electric field, graphene grows vertically instead of horizontally. The MoS₂@3DVG foams with active exposed edges and vertical structure demonstrated the suitability as binder-free electrode for application in Li-ion storage. MoS₂@3DVG foams showed better rate capability than the three-dimensional graphene (3DG, having planar graphene) prepared by the conventional CVD method (Figure 3f). The capacity of MoS₂@3DVG electrode reaches up to ~400 mAh g⁻¹ at a high current density of 3200 mA g⁻¹. Apart from radio frequency plasmas, other plasma source with different frequency like microwave plasmas have also been reported in synthesis of binder-free electrode.^[34–35] For example, Zhang et al.^[36] grew 3D vertically-oriented

graphene nanosheets (GNs) on the graphene aerogel (GA) template using the microwave plasma chemical vapor deposition (MPCVD) method. As-prepared binder-free, lightweight electrode have a high electrical conductivity of ~1000 S m⁻¹. The obtained GA-GN with hierarchical nanoscale structures had large specific surface area ($128 \text{ m}^2 \text{ g}^{-1}$) of hierarchical structures. The unique “edge effect” of GNs that reduced ion diffusion path from the electrolyte to the electrode surface. Thus, the electrodes also exhibited excellent capacitive performance including a high specific capacitance of 245 F g^{-1} and excellent cyclic stability with 92% capacitance retention after 10000 cycles.

In particular, for the synthesis of CNT-based, binder-free electrode, floating catalyst chemical vapor deposition (FCCVD) system with a vertical reaction chamber has been the focus recently. FCCVD is inexpensive and scalable, and can well control the morphology of CNTs or bundles in the thin film,^[37] which is regarded as a potential method for high-yield production of CNT with high purity.^[38–40] Figure 4a shows a typical FCCVD system for CNT synthesis.^[39] In the upper part of the vertical reaction chamber with high temperature, the precursor solution decomposed and formed an aerogel of CNTs which transformed into CNT film at the bottom of the chamber by hydrogen gas. The obtained binder-free and freestanding CNT film electrodes have a large specific surface area of $198 \text{ m}^2 \text{ g}^{-1}$. Majeed et al.^[41] employed the FCCVD method to synthesize SWCNT film decorated with a high content of carbon encapsulated Ni (CENi) nanoparticles. Nickelocene dissolved in toluene solution serves as a catalyst precursor, while the thiophene serves as a growth promoter. During the FCCVD process, single-wall carbon nanotubes (SWCNTs) and carbon-encapsulated Ni nanoparticles grew on the stainless steel (SS)

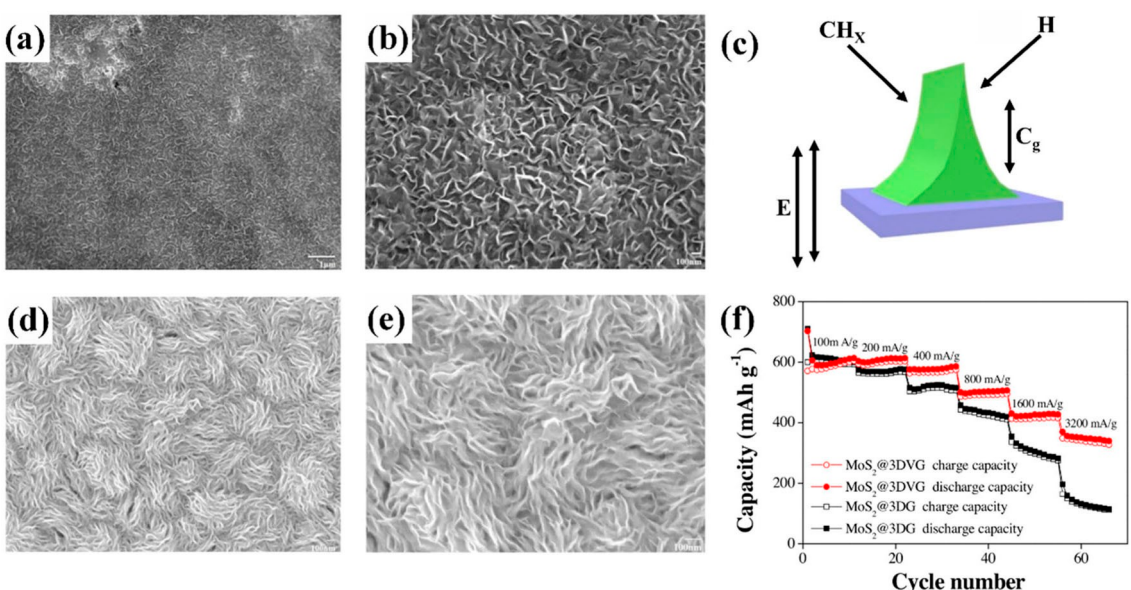


Figure 3. a–b) SEM images of 3DVG nanosheets at different magnification, c) a schematic explanation of the growth model of VG (E = the electric field near the substrate surface; CH_x = gaseous carbon radicals; C_g = growth species diffuse along with a vertical graphene layer; H = hydrogen atoms remove carbon atoms from the solid state), d–e) SEM images of MoS₂@3DVG at different magnifications, and f) the rate stability of the MoS₂@3DVG and MoS₂@3DG (3D-planar graphene foam) electrodes. Reproduced from Ref. [33] with permission. Copyright 2016, Elsevier.

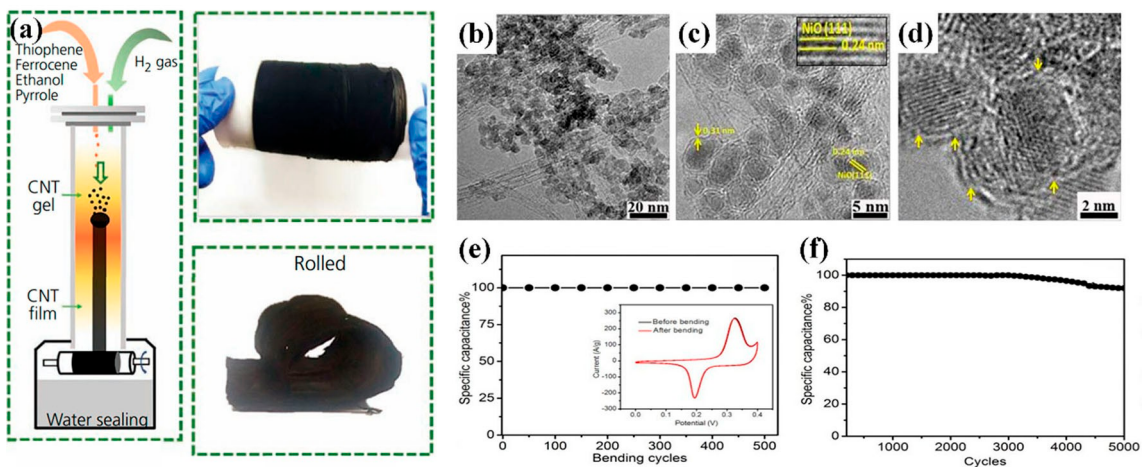


Figure 4. a) Schematic illustration of the preparation of CNT film via FCCVD method and the flexibility of CNT film. Reproduced from Ref. [39] with permission. Copyright 2019, ICE Publishing. b-d) TEM images of CENiO/SWCNT film, e) capacitance retention versus number of bend (the inset shows CV curves of the CENiO/SWCNT film before and after 500 bending cycles), f) stability test of the CENiO/SWCNT film for 5000 cycles. Reproduced from Ref. [41] with permission. Copyright 2017, The Royal Society of Chemistry.

mesh under mixed gas of H_2 and C_2H_4 . After air oxidation, the carbon-encapsulated NiO nanoparticles (CENiO) decorated on SWCNTs was obtained (denoted as CENiO/SWCNT). Figure 4b-d indicates small NiO nanoparticles encapsulated by carbon shells are well and uniformly dispersed in highly conductive SWCNT interconnected networks, enabling efficient electron transfer and electrolyte ion diffusion in the CENiO/SWCNT electrode. The CENiO/SWCNT exhibited both excellent mechanical flexibility (Figure 4e), and capacitive performance including a maximum specific capacitance of 810 F g^{-1} at 30 A g^{-1} and excellent reversible capacity retention of 92% after 5000 cycles (Figure 4f).

2.2. Vacuum Filtration Method

Vacuum filtration a facile and cost-effective method to fabricate binder-free and freestanding film electrodes with good homogeneity and uniform thickness.^[42-43] Generally, the common vacuum filtration method has relatively cheap devices including a Buchner funnel, filter and vacuum system. By filtering different kinds of solutions or dispersions, the various film-based electrode such as CNT film,^[44-45] graphene oxide/MnO₂ composite paper,^[46] activated carbon (AC)/CNT paper,^[47] MXene/CNT paper^[48] and MoS₂-CNT^[49] can be fabricated. For instance, when colloidal dispersion of GO was filtered through a membrane substrate under vacuum, the GO sheets retained on the membrane surface and accumulated to form a GO film, owing to the size of the GO sheets is larger than the size of the membrane pores.^[50] However, the electrical conductivity of GO papers is low due to oxygen-containing functional groups.^[51] For energy storage materials, the GO needs to be reduced by chemical or high-temperature annealing treatments to enable higher conductivity. Yuan et al.^[52] reported a Na₄Mn₉O₁₈ (NMO)-rGO hybrid film which was prepared by a facile vacuum filtration technique, as shown in Figure 5 (a). Briefly, the NMO

and GO suspension, obtaining via dissolving and ultrasonic treatment in deionized water, was filtered through a filter membrane, air-dried, and NMO-GO film was peeled from the membrane to synthesize the NMO-rGO hybrid film via heat treatment. NMO needle-like particles were evenly distributed and anchored on the conductive RGO matrix, which can significantly reduce volume expansion and prevent agglomeration of NMO particles, thereby improving cyclability of the electrodes. A sodium battery was assembled by using NMO-rGO film as cathode and zinc metal as anode in an aqueous electrolyte. The NMO-rGO film delivered a reversible discharge capacity of $\sim 83 \text{ mAh g}^{-1}$ at a current density of 0.1 A g^{-1} , which was 78% higher than the electrode prepared by a slurry casting technique.

Through vacuum filtration method, 2D materials can be easily assembled into flexible self-standing paper-like materials, which can be directly used as flexible binder-free electrodes in energy storage devices.^[53] Transition metal dichalcogenides (TMDCs) such as MoS₂, MoSe₂, WS₂, as new class of 2D materials, attractive applications in electronics and energy storage devices.^[54] Liu et al.^[55] fabricated a N-doped carbon microtubes@amorphous MoS₂/rGO (NCMTs@A-MoS₂/rGO) membrane using the vacuum filtration method. The carbonated willow catkins (N-doped carbon microtubes resources) were used as a substrate to grow amorphous MoS₂ through a hydrothermal process. Then the NCMTs@A-MoS₂ composite film was synthesized via vacuum filtration and a subsequent calcination process (Figure 5b). Due to the cross-linked carbon networks of NCMTs and rGO, NCMTs@A-MoS₂/rGO film shows an electrical conductivity of 0.98 S m^{-1} , which is much higher than that of pure A-MoS₂ ($1.4 \times 10^{-3} \text{ S m}^{-1}$). Galvanostatic Intermittent Titration Technique (GITT) and cyclic voltammetry (CV) analysis indicates that the NCMTs@A-MoS₂/rGO, as a binder-free anode for lithium-ion batteries, displayed better lithium-ion diffusivity than the traditional NCMTs@A-MoS₂ electrode. Figure 5c-d shows that as-prepared binder-free

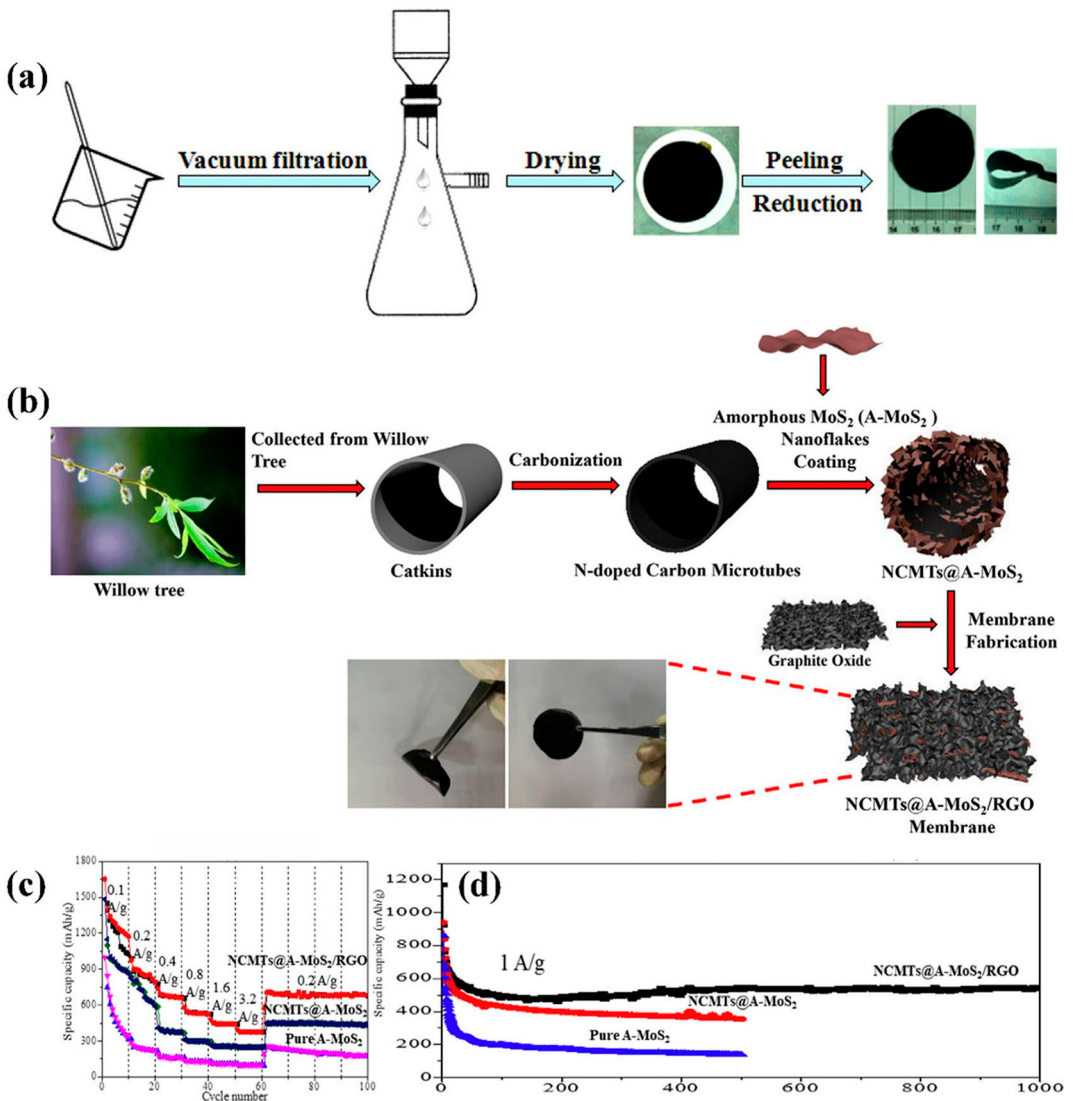


Figure 5. a) Schematics of the NMO-RGO composite synthesis. Reproduced from Ref. [52] with permission. Copyright 2017, Nazarbayev University. b) Schematic illustrations of the synthetic process of NCMTs@A-MoS₂/rGO composite paper, c) rate performance and d) long cycling performance of NCMTs@A-MoS₂/RGO, NCMTs@A-MoS₂ and pure A-MoS₂. Reproduced from Ref. [55] with permission. Copyright 2019, Elsevier.

electrode had both stable cycling stability and excellent rate capability.

As a new type of nanomaterial with unique hollow structure, CNT has good electron transport performance and an ability to form nano-mesh structure.^[56] The addition of CNT can effectively enlarge the interlayer spacing of MXene flakes and prevent its re-stacking. CNT was introduced into MXene via a vacuum filtration method. The obtained sandwich-like MXene/CNT had an enlarged interlayer space which offered fasted diffusion paths for electrolyte ions. As shown in Figure 6a-d, the restacking of MXene nanosheet ($Ti_3C_2T_x$) can be effectively inhibited by addition of CNTs and the obtained sandwich-like MXene/CNT film exhibits good flexibility (see Figure 6e).^[57] In addition, MXene can provide higher capacitance in acid electrolyte stemming from rapid surface redox reaction. Thus, the optimal freestanding flexible MXene/CNT-5% (the mass ratio of CNT: MXene was 5 wt%) illustrated a high capacitance of

300 F g⁻¹ at a current density of 1 A g⁻¹ and capacitance retention ratio of 51% under 1000 A g⁻¹. Figure 6f demonstrates excellent cycle performance with a high capacity retention of 92% after 10000 cycles at 20 A g⁻¹.

2.3. Hydrothermal/Solvothermal Synthesis

Hydrothermal/solvothermal synthesis is another most often used method to prepare binder-free electrodes. Hydrothermal approach has unique advantages due to its precise and versatile morphological control, great flexibility in selection of building material precursors.^[58] Materials normally exhibit higher solubility in water under high pressure and temperature environment in a hydrothermal system.^[59-60] The solvothermal method is analogous to the hydrothermal method, except that the solvent is replaced by a non-aqueous organic solvent.^[61]

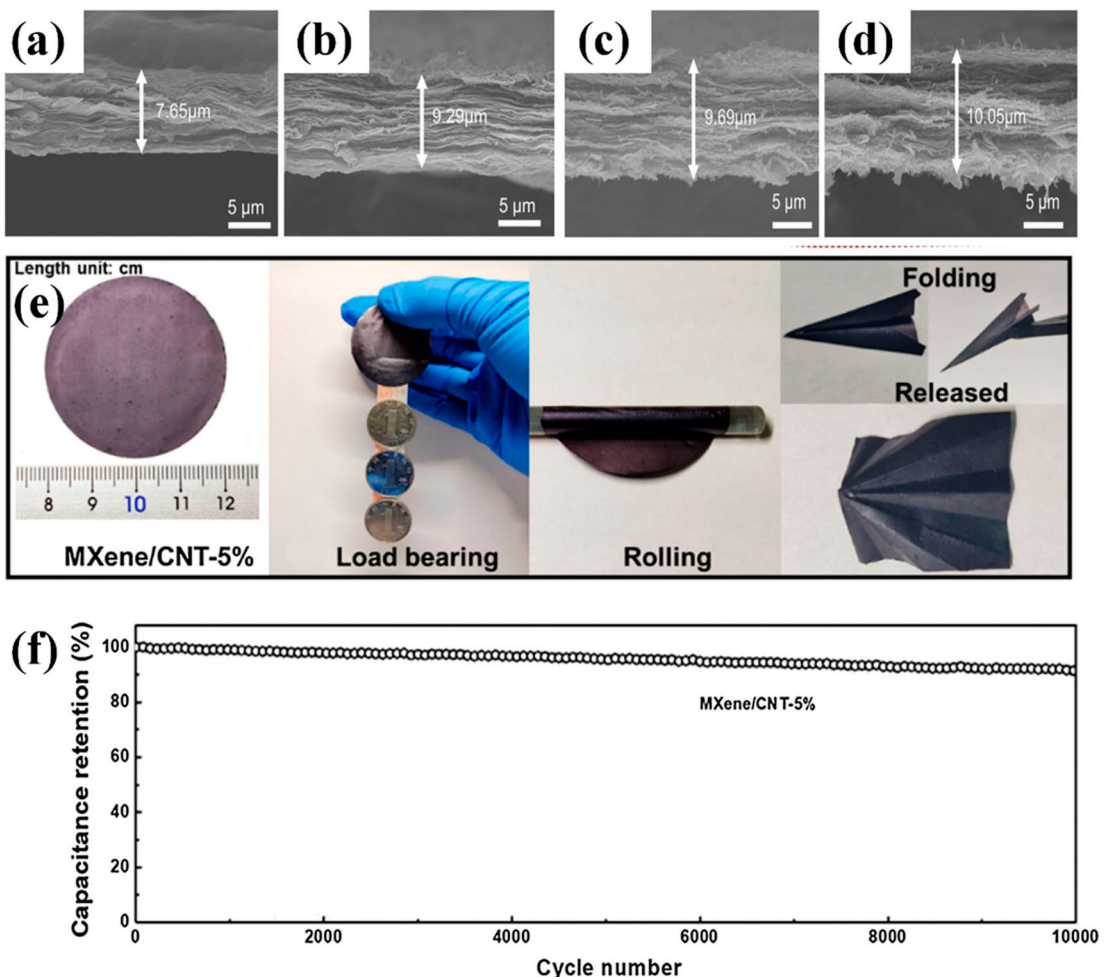


Figure 6. Cross-sectional SEM images of a) MXene, b) MXene/CNT-1 %, c) MXene/CNT-5 %, and d) MXene/CNT-10 % film, e) top view and flexibility test of the MXene/CNT-5 % film, f) cyclic performance at 20 A g^{-1} of the MXene/CNT-5 % film in $1 \text{ M H}_2\text{SO}_4$. Reproduced from Ref. [57] with permission. Copyright 2019, Springer Nature.

Teflon-lined autoclave is the most often used hydrothermal reactor under heated and pressured conditions.^[62] Typically, substrate (e.g., carbon cloth) require further treatment to remove the impurities and/or introduction oxygen-containing groups to make them more hydrophilic and provide suitable nucleation sites. The hydrolysis process and reaction rates can be accelerated under higher temperature and pressure. At the same time, nucleation and crystal growth are also facilitated.^[63] In addition, the introduction of the substrate contributes to directional growth and can provide gaps between the adjacent nanostructures.^[64] Pazhamalai et al. reported that the copper tungsten sulfide (CWS) exhibited almost vertically structures oriented on the surface of Ni foam while the CWS grow without Ni foam has most of plate-like nanostructures. The hierarchical CWS nanostructures grown on Ni foam comprise of both rod- and plate- like structures, which enabled sufficient contact with the electrolyte and efficient ion diffusion within the electrode. The CWS/Ni electrode also provide large electroactive surfaces with abundant active sites. The as-synthesized binder-free electrode with high electroactive surfaces exhibited high specific capacitance (107.9 F g^{-1}) and excellent cyclic stability

over 10000 cycles as asymmetric supercapacitor (ASC, graphene as a positive electrode).

To achieve orderly, high-mass loading and mesoporous Ni–Co–Mn hydroxide nanoflakes (NCMH) on Ni foam, a seed-assisted method was proposed (Figure 7a).^[65] The Ni(OH)_2 nanorod arrays are employed as seeds, which can effectively reduce the crystal size of NCMH and prevents the nanoflake agglomeration. Initially, the urea released NH_3 , then slowly hydrolyzed to NH_4^+ during the hydrothermal process. When the seeds (Ni(OH)_2) reacted with the two products in the solution, the above two-step was accelerated reaction to form more OH^- . Meanwhile, the M^{2+} (Ni^{2+} , Co^{2+} , Mn^{2+}) which released from the nickel nitrate hexahydrate, cobalt nitrate hexahydrate and manganese nitrate tetrahydrate respectively, reacted with OH^- and uniformly deposited on Ni(OH)_2 nanorod seeds to create crystallized NCMH. Orderly grown NCMH can effectively decrease collapse of nanoflakes at high mass loading and promotes contact between active materials and electrolytes. Even at 10 mg cm^{-2} , the NCMH maintained capacity retention of 70% after 1000 cycles at 20 mA cm^{-2} (Figure 7b).

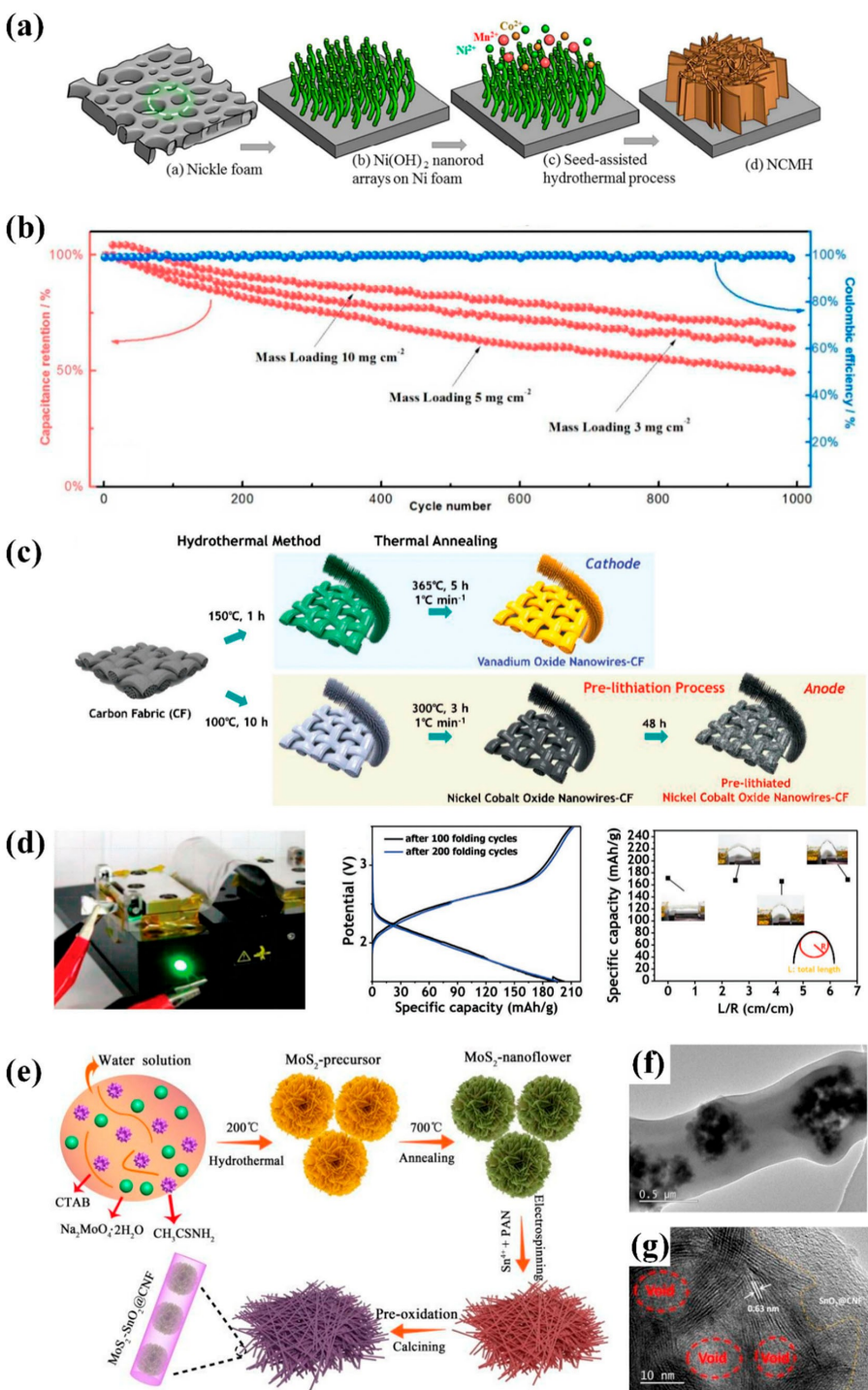


Figure 7. a) The formation mechanism of NCMH, b) the cycling performance of NCMH with different mass loading (measured at 20 mA cm^{-2} in 6 M KOH aqueous solution). Reproduced from Ref. [65] with permission. Copyright 2017, The Royal Society of Chemistry. c) Synthetic routes of nanowire-carbon fabric cathode (V_2O_5 nanowires-CF) and anode (NiCo_2O_4 nanowires-CF), d) bending test of the assembled flexible lithium-ion battery from nanowire-carbon fabric electrodes. Reproduced from Ref. [90] with permission. Copyright 2019, Wiley-VCH. e) Diagrams for the formation of $\text{MoS}_2\text{-SnO}_2\text{@CNF}$ composites and f-g) TEM images of $\text{MoS}_2\text{-SnO}_2\text{@CNF}$. Reproduced from Ref. [91] with permission. Copyright 2019, The Royal Society of Chemistry.

Apart from various metal-based skeletons such as Ni foam,^[66–69] Cu foam,^[70–71] Ti mesh^[72] and stainless steel,^[73] other substrates have also been employed in the hydrothermal/solvothermal processes to synthesize binder-free electrodes.^[74–76] Among them, carbon fibers are one popular

electrode substrate due to their high electrical conductivity, chemical inertness and flexibility.^[77] Carbon fiber-based electrodes have been widely adopted in lithium-sulfur batteries,^[78–79] lithium-ion batteries,^[80–81] sodium-ion batteries,^[82–83] supercapacitors,^[84–85] etc. For instance, Ma et al.^[86] grew hollow

CoMoS₄ nanotubes on the roughness surface of carbon cloth (CC) via a hydrothermal reaction. The formation mechanism of CoMoS₄ is described as follows. Under high temperature and pressure, the urea quickly released OH⁻, leading to the formation of Co(OH)F nanowires in the aqueous solution containing Co²⁺ and F⁻ ions. Then Co(OH)F nanowires were converted into hollow CoMoS₄ nanotubes via a sulfidation treatment. After a facile electrodeposition method, the CoMoS₄@Ni-Co-S was obtained. The assembled ASC device (CoMoS₄@Ni-Co-S//AC) showed an energy density of 49.1 Wh kg⁻¹ at a high power density of 800 W kg⁻¹ and excellent cycling stability with 90.3% retention after 10000 cycles. Owing to wide lithiation/delithiation potential windows, simple synthesis and rich reserves, vanadium pentoxide (V₂O₅) is a popular electrode material.^[87-89] Son et al.^[90] grew V₂O₅ nanowires (cathode) and lithiated nickel cobalt oxide (NiCo₂O₄, anode) nanowires on plasma-treated carbon fabric (CF), respectively, via a hydrothermal and subsequent annealing process (Figure 7c). The plasma-treatment of CF could generate functional groups (such as hydroxyl, carboxyl and carbonyl) which provide firm anchoring and bonding points for active materials on the surface of CF, avoiding detaching during charging and discharging. The nanowires can effectively reduce the stress caused by volume expansion. Using as-prepared electrodes and PEO-based quasi-solid polymer electrolyte, a bendable lithium-ion battery was assembled. The device exhibited a high energy density of 364.2 Wh kg⁻¹. In addition, the device also had excellent mechanical stability. After 200 folding cycles (Figure 7d), its capacity still retained at around 185 mAh g⁻¹ under a current density of 30 mA g⁻¹.

Hydrothermally assembled materials can be encapsulated in electrospun nanofiber-based freestanding film. For example, Chen et al.^[91] synthesized MoS₂-SnO₂@CNF electrode as anode for lithium-ion batteries by hydrothermally grown MoS₂-SnO₂ on electrospun nanofibers, as illustrated in Figure 7e. The MoS₂ nanoflower and amorphous SnO₂ encapsulated into carbon nanofibers (see Figure 7f-g), forming a broad bean shape, which are beneficial for fast ion intercalation and diffusion kinetic reactions. As binder-free anode for Li-ion batteries, it sustained for at least 800 cycles with a stable capacity of 710 mAh g⁻¹ at 200 mA g⁻¹.

2.4. Aerogel Production Process

Aerogel-based electrodes are one important branch of binder-free electrode family. Aerogel production normally involves a sol-gel process to form a monolithic network, followed by supercritical drying or freeze-drying to replace the solvent with air. As a result, aerogel retains the 3D structure with high porosity, large specific surface and lightweight, which is favorable for electrochemical energy storage.^[92]

Graphene oxide (GO) is a suitable precursor for preparing graphene-based aerogels (GA). Because GO has hydrophobic basal plane and hydrophilic oxygen-containing groups, and is able to react covalently with different compounds.^[93] For example, Shen et al. reported a 3D graphene aerogel through a

wet-chemical synthesis process followed by freeze-drying and heat treatment, where Prussian blue (PB) nanocubes were deposited on the 3D GA current collector, serving as cathode of high-performance sodium-ion batteries.^[94] The 3D graphene framework worked as not only conductive network for efficient electron transfer but also mechanical support in the free-standing electrode. In 2012, Jung et al. reported a novel method to assemble 3D aerogels over a wide range of materials. As illustrated in Figure 8a, they firstly prepared well-dispersed, individual nanotube/nanowire/nanosheet suspension. Then under the desired temperature, the solvent was evaporated to form more concentrated suspensions in which van der Waals forces drove nanotube/nanowire/nanosheet to link together to create physical bonds. Finally, aerogels were successfully synthesized after critical point drying (CPD).^[95] By using this method, dilute suspensions including electrochemically exfoliated graphene were evaporated slowly at 313 K to form more concentrated suspensions (gels), following by freeze-drying process, a GA was obtained. It possessed a high specific surface area of 496 m² g⁻¹ and mesopores diameter ranging from 2 to 50 nm.^[96] Then a supercapacitor was constructed by using as-prepared GA as electrodes and IL-FSN (the IL for (1-ethyl-3-methylimidazolium bis(trifluoromethylsulfonyl)imide and FSN for silica nanoparticle) composite polymer as gel electrolyte (Figure 8b-g). At higher temperatures, the addition of FSNs results in the improved thermal stability and enhanced content of the amorphous part of the polymer matrix which is beneficial to ionic conductivity. Moreover, the electrolyte ions can diffuse into the pores of the graphene aerogels with enhanced ion transport kinetics at the electrode/electrolyte interface, leading to good capacitance and rate performance at high temperatures. The high electrochemical performances can be seen from Figure 8h, it maintained 90% capacitance retention after 10000 cycles at 200 °C. In addition, the energy and power densities (calculated using the total mass of devices) can reach at ~17.5 Wh kg⁻¹ and ~160 W kg⁻¹ at 200 °C.

Furthermore, 3D-printing technique is also a novel method to produce GA. For instance, Yao et al.^[97] employed direct ink writing (DIW) method, a most common 3D-printing technique,^[98] to print 3D electrodes using GO ink (Figure 9a). After freeze-drying and annealing, the obtained 3D printed GA underwent a subsequent electrochemical and cleaning processes to introduce oxygen-containing groups on their surface, yielding surface-functionalized 3D-printed graphene aerogel (SF-3D GA) (see Figure 9b-c). The 3D-printed periodic porous structure facilitates ion diffusion, while the oxygen-containing groups on the surface could contribute pseudocapacitance. At the same time, the small pore/channel size is beneficial for high mass loading of active materials in the electrode. Meanwhile, the authors summarized and compared five metrics including mass loading of the electrode materials, Brunauer-Emmett-Teller (BET) areal capacitance, areal capacitance, gravimetric capacitance and rate capability as shown in Figure 9d. In general, although under the same mass load and low current density, the areal and gravimetric capacitances of SF-3D GA was only slightly higher than that of SF-GA. But the rate

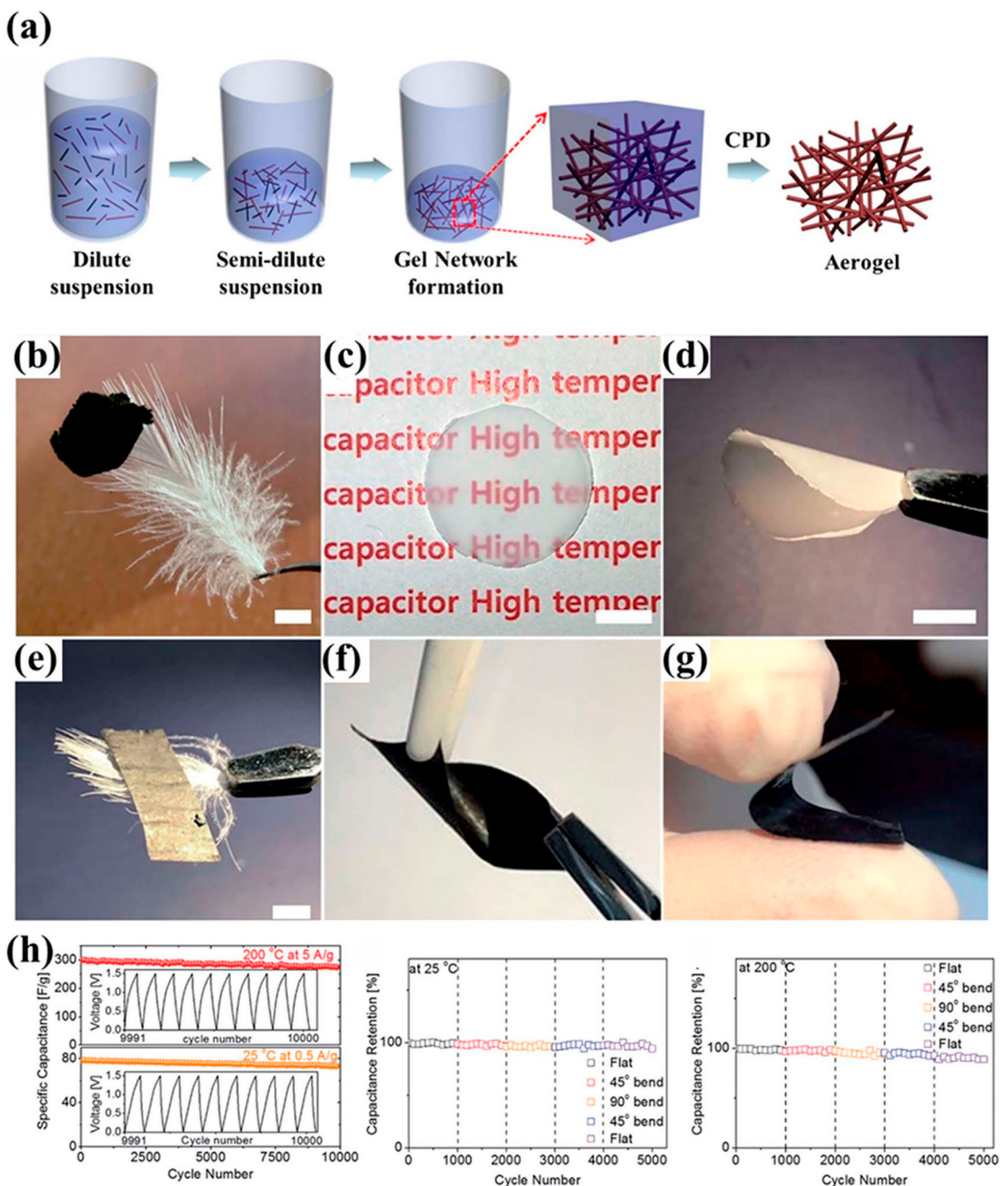


Figure 8. a) The illustration of the production process of gel/aerogel. Reproduced from Ref. [95] with permission. Copyright 2012, The Authors. b) Ultralight GA film on a feather, c-d) semi-transparent and bendable features of the IL-FSN based composite electrolyte, e-g) a ultralight, twistable and bendable supercapacitor device (scale bar is 0.5 cm) made from GA electrodes and h) its cycling performance at room temperature and 200 °C (the inset shows the galvanostatic charge/discharge curves) and capacitance retention under different bending angles at room temperature and 200 °C. Reproduced from Ref. [96] with permission. Copyright 2020, The Royal Society of Chemistry.

capability of SF-3D GA was significantly better than SF-GA, which confirmed the significant role of 3D printing structure for enhancing the capacitance of high mass loading electrodes at high current densities. Then an asymmetric supercapacitor was assembled by using the SF-3D GA as the negative electrode, MnO₂ electrodeposited 3D GA as the positive electrode. With a voltage window of 2 V, the assembled device exhibited a capacitance retention of 93% after 100000 cycles at 100 mV s⁻¹, and had energy density of 0.65 mWh cm⁻² at high power density of 164.5 mW cm⁻², demonstrating excellent electro-

chemical performances (Figure 9e-f). Under the high mass loadings 24.8 mg cm⁻², the volumetric energy and power density can reach up to 1 mWh cm⁻³ and 100 mW cm⁻³, respectively.

2.5. Electrospinning

Electrospinning is another method to prepare binder-free and freestanding film electrodes which consist of randomly inter-

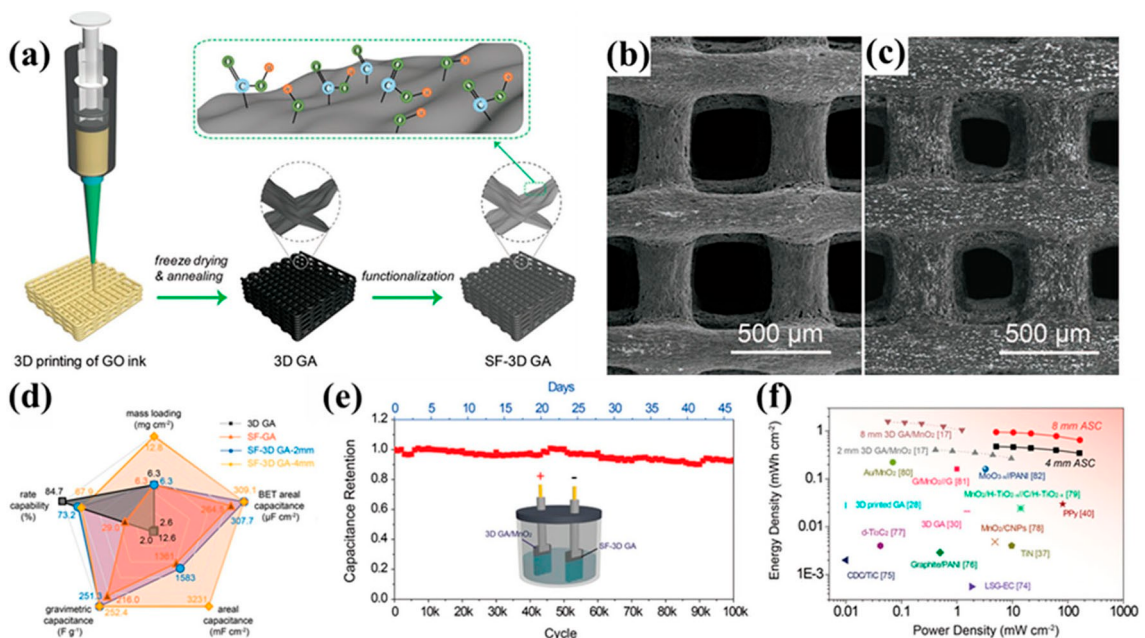


Figure 9. a) Schematic illustration of preparing process of SF-3D GA. SEM images of b) 3D GA and c) SF-3D GA. d) A radar chart which compares five metrics of 3D GA, SF-GA, and SF-3D Gas electrode. e) long-term stability of the 3D GA/MnO₂//SF-3D GA asymmetric supercapacitors. (Inset: illustration of the 3D GA//MnO₂//SF-3D GA device) f) Ragone plots of the 3D GA/MnO₂//SF-3D GA device and various other electrochemical energy storage devices. Reproduced from Ref. [97] with permission. Copyright 2020, The Authors.

laced nanofibers.^[99] This technique requires polymer precursor dispersing in aqueous or organic electrolyte or melting. At the same time, various nanoparticles (e.g., conductive enhancer or electrode materials) could be added into the mother polymer dispersion or melt to spin hybrid nanofibers.^[100–102] However, the agglomeration or re-stacking of particles or two-dimensional sheets in the composite solution may cause beading or inconsistencies on the fiber. A stable and homogenous solution for electrospinning is vital for scale-up.^[103] In a typical electrospinning process, a solution is firstly fed through a spinneret. When a sufficiently high voltage is applied, the solution in the spinneret becomes charged. Meanwhile, the electrostatic repulsion counteracts the surface tension, and at a critical point, the droplet emits a jet of liquid which is called Taylor cone,^[104–106] as illustrated in Figure 10a. When the jet flies to the collector which is several centimeters away from the spinneret tip, the solvent evaporates and polymer nanofibers finally deposit on the surface of the collector^[99] (see Figure 10b). Besides the intrinsic properties of solutions like concentration and viscosity, the operating parameters including flow rate, electric field intensity and environmental factors such as air humidity and temperature also influence the morphology of the electrospun fibers.^[107]

Chen et al.^[108] reported a freestanding and foldable carbon nanofibers (FCNFs)-based flexible anode for LIBs using a Zn(Ac)₂-assisted electrospinning-peroxidation-carbonization process, as illustrated in Figure 10c. During the electrospinning process, Zn atoms and the N atom of nitrile group form Zn–N bond, which could decrease the crystallinity of PAN nanofibers and thus enhance the flexibility of PAN nanofibers. To obtain a freestanding electrode, the subsequent heat treatment for

electrospun fibers is necessary. Under the peroxidation process at ~250 °C, CH₃COO• released from Zn(Ac)₂ and C atoms of the CN groups form ladder polymer which increase the stability of PAN nanofibers. During the carbonization process, ZnO (decomposed from Zn(Ac)₂) creates defects and pores in foldable nanofibers, which significantly increases the specific surface area.

Besides Li-ion batteries, electrospun nanofiber-based electrodes have also been widely used in other battery systems.^[99,109] For example, the mass loading of electrospun Na_{0.7}FePO₄F@C nanofiber film can achieve 2.3–2.7 mg cm⁻² by changing electrospinning time.^[110] As a binder-free cathode for sodium-ion storage, it delivered high capacity retention of 85% after 2000 cycles at 620 mA g⁻¹. As for the anode of the Na-ion batteries, the hard carbon facilitates sodium ion desorption and insertion reactions in carbon structure. Chen et al.^[111] proposed a loofah-like nitrogen-doped hollow carbon nanofibers (NHCNFs) through hard template route via electrospinning, as illustrated in Figure 10d. In this work, the used colored acrylic yarn was employed as the carbon and nitrogen-doped source and nickel acetate tetrahydrate is used as a hard template to produce micropores through acid treatment. Theoretical simulation indicated the N-doping included pyrrolic and pyridinic was beneficial for sodium adsorption. The continuous hollow pores structure in carbon fibers (Figure 10e) accelerated diffusion of Na ions, offering 156 mAh g⁻¹ under the current density of 15 A g⁻¹ after 10000 cycles (Figure 10f).

The coaxial electrospinning is a facile process to synthesize core-shell or hollow nanofibers. As for the core-shell structured fibers, the shell is a protective layer or support /substrate to maintain the function of core material.^[112] The advantages for

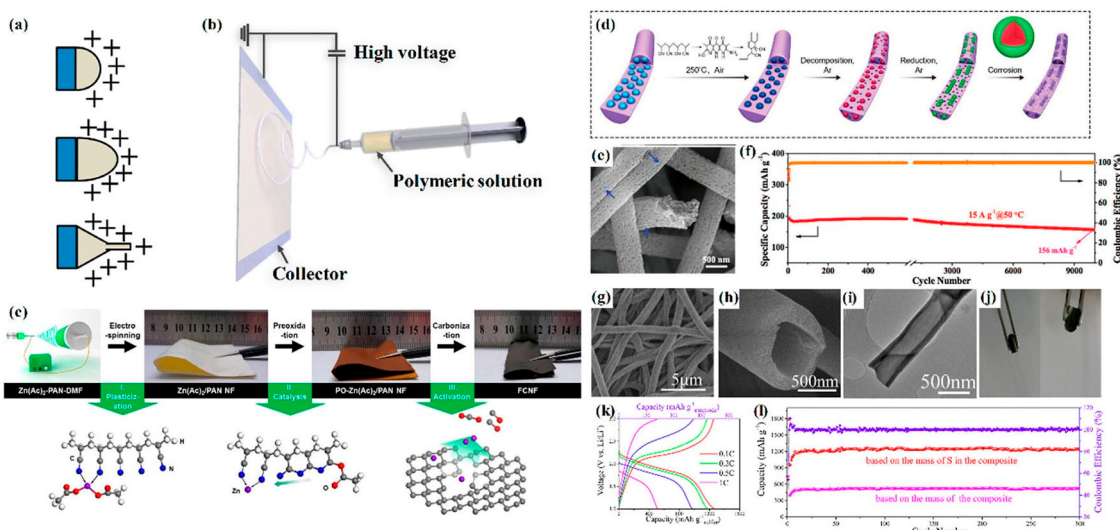


Figure 10. a) Schematic of Taylor cone formation. Reproduced from Ref. [105] with permission. Copyright 2019, The Authors. b) Schematic diagrams for the electrospinning. c) Schematic illustration of the formation mechanism of FCNF. Reproduced from Ref. [108] with permission. Copyright 2017, The Royal Society of Chemistry. d) Schematic diagrams of preparation procedure of nitrogen-doped hollow carbon nanofibers (NHCNFs). e) SEM image of NHCNFs. f) Cycling performance under a current density of 15 A g^{-1} . Reproduced from Ref. [111] with permission. Copyright 2020, Wiley-VCH. g-h) SEM and i) TEM images of H-SPAN, j) flexibility of H-SPAN films, k) rate capability and l) long-term cycling performance of H-SPAN electrode. Reproduced from Ref. [115] with permission. Copyright 2019, Elsevier.

the hollow nanofibers involve high surface-to-volume that offers numerous electrochemically active sites and provides fast pathways for electron transport.^[113–114] In a coaxial electrospinning process, different solutions can be driven in a coaxial spinneret to form coaxial nanofibers.

Interestingly, when the internal polymer is eliminated in the core-shell structure, a hollow structure fiber can be synthesized. For example, the PEO core in the core-shell coaxial nanofibers is removed by ultrasonic treatment to make hollow tubular nanofibers, then H-SPAN (sulfurized polyacrylonitrile film with hollow tubular nanofibers) was obtained through the sulfurized process, as displayed in Figure 10g-j. Owing to the hollow construction, the H-SPAN achieved 41.18% S loading content of the whole electrode and sufficient contacted between electrode and electrolyte. Figure 10k-l indicated a stable capacity of about $514.7 \text{ mAh g}_{\text{electrode}}^{-1}$ at 0.1 C after 300 cycles for the Li-S batteries.^[115]

2.6. Electrophoretic and Electrochemical Deposition

Electrophoretic deposition (EPD) is a coating process in which colloidal particles suspended in a liquid medium migrate under electric field and are deposited on an electrode with opposite charge.^[116–117] The mobility of colloidal particles is influenced by several factors including the dielectric constant and viscosity of the fluid, the potential gradient and the zeta potential of the colloidal particles.^[118] The above parameters could be described via the Henry equation [Eq. (1)]:

$$\mu = \frac{2 \epsilon_0 \epsilon_r \zeta}{3 \eta} f(\kappa_r) \quad (1)$$

where μ the electrophoretic mobility, ϵ_0 is the permittivity of vacuum, ϵ_r the relative permittivity of the solvent, ζ is the zeta-potential, η the viscosity of the suspension and $f(\kappa_r)$ the Henry correction function.^[119] The electrophoretic mobility of the particles suspended is inversely proportional to the viscosity of the liquid, whereas it is in direct relation with the zeta potential.

The electrophoretic mobility of suspended particles is inversely proportional to the viscosity of the liquid, and is directly related to the zeta potential of the suspension.

In general, to synthesize high-performance electrode materials via EPD method, there are several parameters should be optimized and post-treatments should be implemented:^[118,120–121] (a) operation conditions such as applied voltage, inter-electrode distance and deposition time; (b) characteristics of a suspension like the concentration of the colloidal particles and charging/stabilizing agents; (c) subsequent heat treatment process.

Li et al.^[122] reported a binder-free electrode which was prepared by electrophoretic depositing black phosphorus/graphene (BP/G) heterostructure on the stainless steel piece, as illustrated in Figure 11a. It is worth noting that the longer EPD time is not helpful for the low electrophoretic mobility graphene solution to deposit on stainless steel electrode. The BP/G anode demonstrated a capacity of $648 \text{ mAh g}_{\text{total}}^{-1}$ after 100 cycles at 100 mA g^{-1} in a Na-ion battery. Besides metal sheets, carbon-based film could also be used as EPD substrate. Recently, a special designed coaxial cylindrical electrode was reported to assemble vertically aligned carbon nanotubes on carbon fiber (VACNT/CF).^[123] Figure 11b illustrated the inner electrode was CF filament and outer electrode was aluminum alloy tube. According to the above mentioned, several parameters should be optimized when assembling the materials via

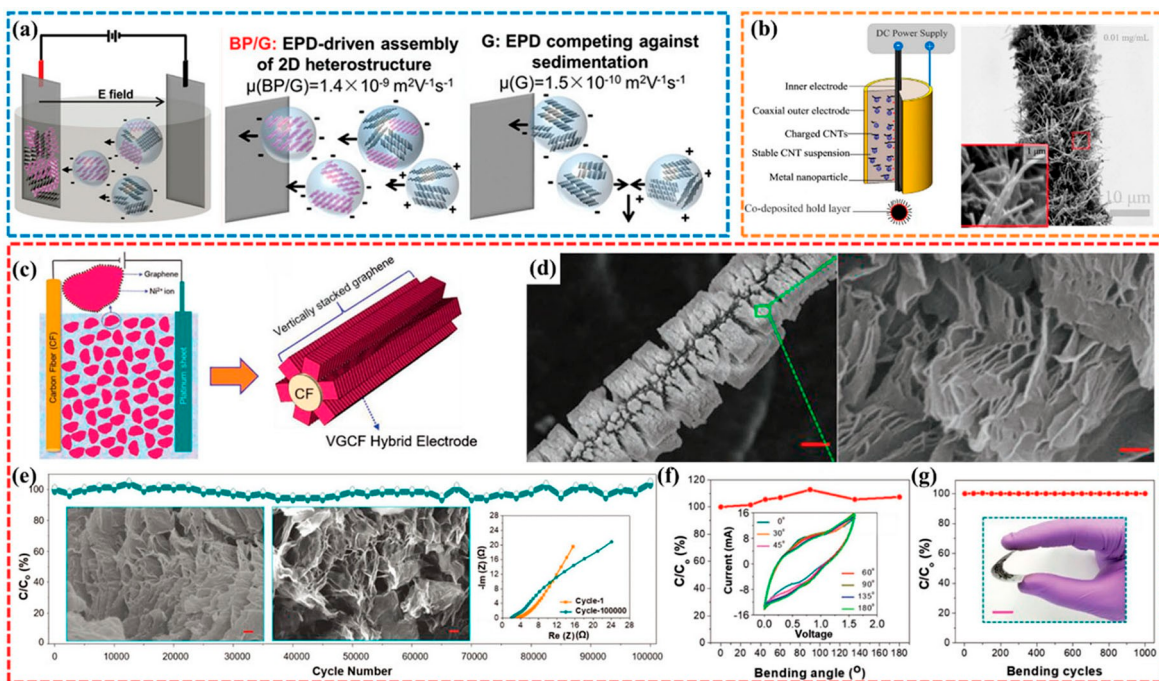


Figure 11. a) Schematic illustration of the EPD process (left) and proposed deposition mechanism (right) of BP/G and G. Reproduced from Ref. [122] with permission. Copyright 2018, the Royal Society of Chemistry. b) Schematic of electrode arrangement in a coaxial electrode and SEM of VACNT/CF electrode. Reproduced from Ref. [123] with permission. Copyright 2019, Elsevier. c) Simplified schematic of the preparation process of VGCF hybrid electrode. d) SEM images of VGCF hybrids. e) specific capacitance retention plot for the VGCF hybrid electrode; SEM images of the VGCF hybrid electrode at before (left) and after completing 100000 cycles (middle, scale: 200 nm) and Nyquist plot of the VGCF hybrid electrode before and after cycling (right), f) capacitance retention at different bending angles (inset: CV curves at different bending angles obtained at a scan rate of 100 mV s⁻¹) and g) capacitance retention for 1000 bending cycles (inset: digital photograph showing the VGCF ASSC bend at an angle of 90°, scale bar: 1 cm) of VGCF ASSC. Reproduced from Ref. [124] with permission. Copyright 2019, Wiley-VCH.

EPD method. As for characteristics of a suspension, the high ϵ_r and low η are beneficial for the fast electrophoretic mobility (based on the Henry equation). Therefore, the acetonitrile (ACN), the high relative permittivity of 37.5, low surface tension (19.10 mN/m at 20°C) and viscosity (0.37 cP at 20°C), was an excellent dispersion medium compared with other solvents (chloromethane (TCM), tetrahydrofuran (THF), isopropyl alcohol (IPA), ethyl alcohol (EA)). About operating conditions, the excessive voltage (90 V), too long time (60s) and high concentration (0.01 mg mL⁻¹) caused the crowding deposition of multilayered CNTs arrays. Thus, optimized parameters were suggested employed ACN as the dispersion medium, including a concentration of 0.01 mg mL⁻¹ MWCNTs (110–170 nm), 30 V deposition voltage and deposition time of 20 s.

Furthermore, as schematically depicted in Figure 11c, the Cherusseri et al.^[124] proposed a normal EPD process to synthesize the vertically aligned graphene-carbon fiber (VGCF) hybrid electrode, which can effectively avoid the stacking of graphene sheets. Meanwhile, by introducing additives, nickel nitrate hexahydrate, in the electrophoretic deposition process, the formation of α -Ni(OH)₂ nanoparticles and oxygen-containing surface functional moieties help the graphene electrodes to exhibit faradaic charge storage and improve specific capacitance of the electrode. The Figure 11e indicated the VGCF hybrid electrode delivered maximum gravimetric capacitance of 333.3 F g⁻¹ at a scan rate of 3 mV s⁻¹ in 1 M H₃PO₄ aqueous electrolyte, and retained ~100% of its initial capacitance after

100000 cycles at 100 mV s⁻¹. The two identical VGCF was assembled fully flexible all-solid-state supercapacitor (ASSC) delivered a high gravimetric energy density of 76 Wh kg⁻¹, and an excellent bendability with 100% capacity retention after 1000 bending cycles (see Figure 11f–g).

In the EPD process, the charged particles dissolving in the organic electrolyte deposit on the surface of the electrode. As for the electrochemical deposition (ED), the ions in aqueous solution coat on the cathode under the electric field, which is similar to electrophoretic deposition.^[125] To get a desired range of nanometers during the electrodeposition process, various conditions such as bath composition, pH, temperature, and current density are needed to consider.^[126]

Nagaraju et al.^[127] optimized the disposition time to generate moderate quantities of OH⁻ ions, were from nitrate ions and the gradual decomposition of hexamine, then reacted with Mn²⁺ ions and formed MnO₂-NS-decorated MnO₂ hexagonal nanoplate arrays (MnO₂ NSs@MnO₂ HNPAs) onto the cleaned CC. The CC fibers were fully covered with MnO₂ NSs@MnO₂ HNPAs, as shown in Figure 12a–b. While CC has ideal flexibility, it still has the disadvantage of low conductivity compared to conventional metal electrodes. In order to tackle this problem, Sekhar et al.^[128] employed the Ag NWs on CC (Ag@CC) via dip-coating approach as the electrochemical deposition substrate. Then deposited nickel-cobalt layered double hydroxide nanosheets on Ag NWs-fenced carbon cloth (NC LDH NSs@Ag@CC) as a binder-free electrode. Briefly, the nitrate (NO₃⁻) ions, in the

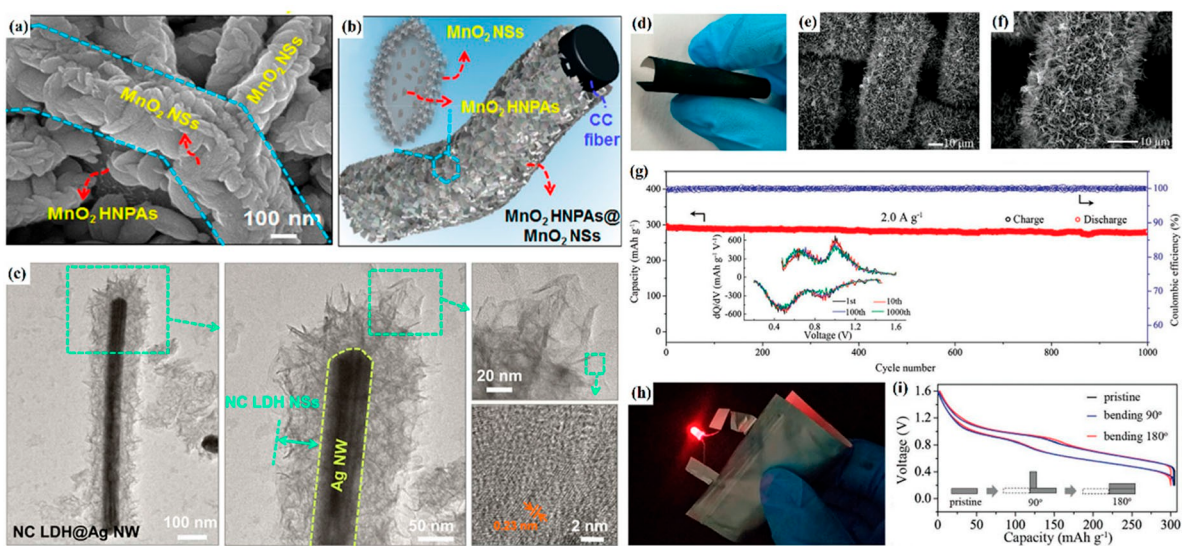


Figure 12. a) SEM images of the MnO_2 NSs@ MnO_2 HNPAs on the CC, b) schematic representation of the hierarchical MnO_2 NSs@ MnO_2 HNPAs on single CC fiber. Reproduced from Ref. [127] with permission. Copyright 2016, Elsevier. c) TEM images of the NC LDH NSs@Ag@CC. Reproduced from Ref. [128] with permission. Copyright 2017, Elsevier. d) A digital image of the flexible and binder-free VOH electrode, e-f) SEM images of the VOH nanobelts, g) long-cycling stability at 2.0 A g^{-1} , the inset shows the selected dQ/dV curves of the VOH cathode for the 1st, 10th, 100th, and 1000th cycles, h) digital photo of a flexible soft-package battery and i) typical discharge/charge curves under the flat state, as well as the 90° and 180° bending states. Reproduced from Ref. [129] with permission. Copyright 2019, Wiley-VCH.

aqueous solution of nickel nitrate and cobalt nitrate, had hydrolysis reaction and formed OH^- ions on the exterior surface of the Ag@CC electrode. Then bimetallic ions (Ni^{2+} and Co^{2+}) rapidly reacted and deposited NC LDHs on the Ag@CC. Figure 12c indicated NC LDH NSs completely covered the Ag NWs, which the interconnected network can effectively diffuse the electrolyte ions into the NSs (battery-type electrochemical behavior materials) and released electrons rapidly move to Ag@CC substrate. The binder-free electrode NC LDH NSs@Ag@CC and AC electrode was assembled as flexible asymmetric supercapacitor, exhibiting a capacitance retention of 88.1% after 2000 cycles at 5 mA cm^{-2} .

Zhang et al.^[129] reported the $\text{V}_5\text{O}_{12} \cdot 6\text{H}_2\text{O}$ (VOH) nanobelt grown *in situ* on the stainless-steel mesh via ECD. They optimized the electrodeposition times as 5 h, the VOH nanobelt homogeneously grew on the surface of stainless-steel fibers, as presented in Figure 12d-f, and the thickness controlled at 6.5 μm . The VOH with nanoscale morphology has large interlayer distance for efficient Zn^{2+} diffusion. At the same time, electrostatic interactions between Zn^{2+} cations and the host framework anions were shielded by the structural water molecules, ensuring stable layered structure. As demonstrated in Figure 12g, the as-prepared VOH nanobelt cathode delivered capacity retention of 94% over 1000 cycles at 2.0 A g^{-1} in aqueous Zn-VOH batteries. Furthermore, a flexible quasi-solid-state Zn-VOH battery employing the VOH as a cathode and Zn foil as anode displayed a stable capacity of $\approx 300 \text{ mAh g}^{-1}$ under different bending states as proposed in Figure 12h-i.

2.7. Selection of the Synthesis Approaches

Regarding the CVD, electrospinning and the electrochemical deposition, they have great potential in preparation of high-performance binder-free electrodes and the large-scale production due to high controllability and purity, and good repeatability. In the past 40 years, CVD has been widely used in industry such as the coating technology for thin-film production.^[15] Moreover, the CVD can control the nucleation and crystal growth at the atomic scale to obtain certain film thickness and uniformity morphology. But it commonly requires a high-temperature reaction environment, partial pressure of reactants, evaporation rate and precursors, which result in high cost could increase the difficulty of industrialization^[21] and limit large-scale application. As for electrospinning, Inovenso Inc. made a production line to achieve scale production, which consists of 110 needles and is able to produce non-woven mat with a width of 1.0 m and has a capacity of 5 kg/day for nanofiber production.^[130] However, fabrication of NFs with diameters less than 10 nm and low production rate still need to be tackle.^[131]

The electrophoretic and electrochemical deposition and hydrothermal/solvothermal have the same advantage that commonly requires one step to synthesize binder-free electrode, which is facile and economical. The additional benefits involving comprising inexpensive experimental facility,^[132] room temperature operating conditions, high efficiency and easy scaling up to large sizes,^[133] prompt EPD and ED has the potential to scale up.^[134] In particular, the side reaction affects the purity of the materials obtained by EPD and ED, which cannot be ignored. In the matter of hydrothermal/solvothermal, several experimental parameters including reagent type, reac-

tant concentration, surfactants, time and temperature will influence the crystallinity, morphology and size of the obtained materials.^[63] Moreover, the long reaction time (several hours to several days) and the uneven temperature distribution in the autoclave will affect uniformity and repeatability of the materials.

The vacuum filtration method and aerogel production can fabricate homogeneous carbon frameworks with active materials for binder-free electrode by adjusting facile parameters, which is a feasible strategy for the experimental research. Meanwhile, prepared 3D conductive network (as a 3D current collector) involves high-performance carbon materials with chemical stability and high contact area, enabling rapid transport of ions/electrons. The ordinary vacuum filtration method has relatively inexpensive devices composing of a Buchner funnel, filter and vacuum system. So far, these filter membranes such as anodic aluminum oxide (AAO) filter membrane, PVDF membrane, PTFE membrane have been reported for synthesizing freestanding films.^[135] When the membrane is several hundred microns thick, the blocking effect slows the rate of the vacuum filtration process.^[136] In order to facilitate the manufacture of aerogel and reduce its cost, novel synthetic processes and new drying methods have made progress.^[137] For example, 3D printing is emerging as a promising processing route to fabricate GAs with several and complex shapes without flake aggregation.^[93] Nevertheless, the expensive raw materials such as single-wall carbon nanotubes, high-quality thin graphene lead to high production costs. That raises the question of whether it is a suitable investment to prepare high-performance binder-free electrodes at a high-cost.

Notably, the high-performance and binder-free electrodes can be achieved by integrating multiple methods, which is not limited to only one method. For example, the high purity carbon materials could be obtained by CVD or electrospinning method, then unique nanosheets with specific orientations are deposited *in situ* via electrophoretic and electrochemical deposition. Based on the reviewed articles, almost every synthesis can be applied in the SCs and batteries. Apart from reviewed materials, the most materials including metal oxides (such as TiO_2 ,^[138] Fe_3O_4 ,^[139] LiCoO_2 ^[140]), metal hydroxides ($(\text{Ni(OH})_2$,^[141]

$\text{Co(OH})_2$,^[142] etc.), metal carbides (TiC ,^[143] $\text{Fe}/\text{Fe}_3\text{C}$,^[144]) can be fabricated via a specific method. With regards to vacuum filtration and aerogel production, the used raw materials rely on the high-performance carbon materials such as CNT, rGO. Thus obtained composites regularly possess high specific surface area, high conductivity and flexibility, which meets requirements of SCs. Meanwhile, the above two methods can effectively mix with other materials (such as MXene, MoS_2 , MnO_2), becoming composites that can employ in batteries. It is a challenge to directly encapsulate MXene in fiber as a supercapacitor electrode by electrospinning. Because of the flakes are trapped within polymer fibers, so the content of MXene must be high to make the fiber conductive.^[145] Significant advantages and disadvantages of 6 synthesis approaches and their applications are shown in Table 1.

3. Summary and Outlook

Binder-free electrode materials exhibit unique advantages compared to conventional electrodes for electrochemical energy storage applications. They include: (1) high mass loading of active materials, (2) well interconnection between active materials themselves and current collectors, (3) high utilization rate of active materials (addressing the “dead mass” issue) and (4) efficient electron and ion transportation within the electrodes, etc.

We have overviewed recent research advances in exploring various approaches for fabricating well-crafted binder-free electrodes, including (1) CVD, (2) vacuum filtration, (3) hydrothermal/solvothermal, (4) aerogel production, (5) electrospinning and (6) electrophoretic and electrochemical deposition. At the same time, the mechanisms of these approaches and performance-determined factors are summarized. Significant achievements regarding binder-free electrodes for rechargeable batteries and supercapacitors have been highlighted (see details in the main text and Table 2).

Although significant research efforts have been devoted to creating high-performance binder-free electrodes using various fabrication approaches, many challenges remain. In our view,

Table 1. The feature comparison of synthesis approaches and the application.

Technology	Advantages	Disadvantages	Applications
CVD	Can be precisely controlled, obtained high purity materials with good uniformity morphology	Usually need for high temperature, high-cost	SCs and batteries
Vacuum filtration	Simple and operable, self-supporting material, relatively inexpensive devices	Currently only in the laboratory stage, high-cost raw materials	SCs and batteries
Hydrothermal/ solvothermal	Various uniformity morphology can be obtained by adjusting parameters	Difficult to control precisely resulting in poor repeatability	SCs and batteries
Aerogel production	Obtain high porosity and lightweight materials	The Freeze-drying process is time-consuming high-cost raw materials	SCs and batteries
Electrospinning	Good repeatability, a simple approach to fabricate nanofibers.	Subsequent heat treatment process affects flexibility	Mostly for batteries
Electrophoretic and electrochemical deposition	Yield uniform and designed shape coatings on substrates, the controllable deposition process at room temperature	A side reaction could occur, the stability of the suspension and high electrophoretic mobility is required	SCs and batteries

Table 2. Different preparation methods for binder-free electrode materials and electrochemical performance.						
Method	Materials	Substrate	Cycling performance	Capacity retention	Application	Ref.
CVD one-step	CNT@FP	CNT	~ 150 mAh/g after 100 cycles at 20 mA/g	98 %	Cathode for NIBs	[26]
CVD one-step	Ni ₃ S ₂ @NC	Ni foam	~ 368 mAh/g after 100 cycles at 1000 mA/g	91 %	Anode for LIBs	[27]
PECVD, hydrothermal	MoS ₂ @3DVG	Ni foam 3DVG	670 mAh/g after 30 cycles at 100 mA/g	99 %	Anode for LIBs	[33]
MPCVD	GA-GNs	GA	245 F/g after 10000 cycles at 1000 mA/g	92 %	SC	[36]
FCCVD	CNT films	No	11.60 mg/g after 4 cycles	N/A	Capacitive deionization	[39]
FCCVD, heat treatment	CENiO _{7y} /SWCNT	SS mesh	1422 F/g after 5000 cycles at 3000 mA/g	92 %	SC	[41]
Hydrothermal, vacuum filtration	NMO-RGO	No	29.4 mAh/g after 160 cycles at 200 mA/g	N/A	Cathode for Re-HABs	[52]
Solvothermal, vacuum filtration, heat treatment	NCMTs@A-MoS ₂ /RGO	No	544 mAh/g after 1000 cycles at 1000 mA/g	~ 71 %	Anode for LIBs	[55]
Wet chemical synthesis, vacuum filtration	MXene /CNT	No	after 10000 cycles at 20000 mA/g	92 %	SC	[57]
Hydrothermal	CWS/Ni	Ni foam	107.9 F/g after 10000 cycles at 0.75 mA	92.1 %	ASC	[64]
Hydrothermal	NCMH	Ni foam	759.8 μAh/cm ² after 1000 cycles 20 mA/cm ²	70 %	SC	[65]
Hydrothermal, electrochemical deposition	CoMoS ₄ @Ni-Co-S	CC	after 10000 cycles at 1000 mA/g	90.3 %	ASC	[86]
Hydrothermal, thermal annealing	VONW-CF	CF	~ 125 mAh/g after 100 cycles at 100 mA/g	~ 83 %	Full LIBs	[90]
Hydrothermal, annealing, Electrospinning, annealing	NCNW-CF MoS ₂ -SnO ₂ @CNF	No	710 mAh/g after 800 cycles at 2000 mA/g	~ 100 %	Anode for LIBs	[91]
Wet-chemical synthesis aerogel production process	3D GA	No	~ 270 F/g after 10000 cycles at 5000 mA/g at 200 °C	~ 90 %	SC	[96]
3D print, aerogel production process, annealing treatment	SF-3D GA	GA	after 100000 cycles at 100 mV/s	93 %	ASC	[97]
Electrospinning, carbonization	FCNF-3/4	No	630 mAh/g after 100 cycles at 200 mA/g	~ 83 %	Anode for LIBs	[108]
Electrospinning, carbonization	Na ₂ FePO ₄ F@C	Al foil	~ 60 mAh/g after 2000 cycles at 620 mA/g	85 %	Cathode for NIBs	[110]
Electrospinning, carbonization acid treatment	NHCNFs	No	156 mAh/g after 10000 cycles at 15000 mA/g	~ 95 %	Anode for NIBs	[111]
Coaxial electrospinning, carbonization sulfurized treatment	H-SPAN	No	514 mAh/g after 300 cycles at 0.1 C 295 mAh/g after 200 cycles at 0.1 C	~ 100 % ~ 78 %	Cathode for Li-S Cathode for Na-S	[115]
Electrophoretic deposition	BP/G	SS foil	1297 mAh/g after 100 cycles at 100 mA/g	~ 55 %	Anode for NIBs	[122]
Electrophoretic deposition	VGCF	CF	after 17000 cycles at 100 mV/s	99.4 %	ASSC	[124]
Electrochemical deposition	MnO ₂ NSs@MnO ₂ HNPs	CC	after 5000 cycles at 1500 mA/g	N/A	SC	[127]
Electrochemical deposition	NC LDH NSs@Ag@CC	Ag@CC	after 2000 cycles at 5 mA/cm ²	88.1 %	ASC	[128]
Electrochemical deposition	VOH	SS mesh	~ 280 mAh/g after 1000 cycles at 2000 mA/g	94 %	Cathode for aqueous zinc batteries	[129]

the following research topics are critical to realizing their practical applications.

3.1. Enhancement of Long-Term Stability

Compared with the traditional slurry system, the binder-free electrode has better electrochemical performance. Guarantees the active materials are uniformly anchored on the support material to prevent the agglomeration and reduce the volume

expansion during cycles.^[53] However, it is still a challenge to assemble a binder-free energy storage device with high energy density, excellent stability and high mass load (> 10 mg cm⁻² for commercial applications). Especially, multiple design factors involving the choice of active materials, current collectors, the type of electrolyte, the interface properties of electrolyte-electrode will affect the energy density and cycle stability.^[146] For example, the cathode materials such as the Li-rich layered oxides, $\text{Li}_{1+x}\text{M}_{1-x}\text{O}_2$ (M is a transition metal), have irreversible local structural transformations due to oxidation of oxygen

during the reaction, which limit stability and result in voltage decay.^[147–148] Furthermore, supercapacitors and batteries require electrolytes have an extended electrochemical stability window.^[149] And a stable electrolyte-electrode interfaces in batteries is crucial for stable, long-term battery operation.^[150] Therefore, the *in situ* technologies, such as *in-situ* TEM, Cryogenic TEM and *in-situ* X-ray diffraction, and simulation software including DFT and COMSOL Multiphysics simulation may be powerful tools for understanding the fundamental issues. Besides, the reasonable design structural and further optimization of binder-free electrode is required. For instance, novel active materials involving 2D MXenes and 3D materials such as MOF-derived 3D structure can be designed and synthesized reasonably to enable large surface areas, excellent permeability with electrolyte and more surface-active sites.

3.2. Further Incensement of the Utilization Rate of Active Material

Based on the reviewed articles, most electrodes have low-level mass loading of active materials, which pales into insignificance for the commercial application (above 10 mg cm⁻²^[135]) and plenty of related works need to be complete.

Future research that maximizes the utilization rate of active material needs to be conducted. Materials that have specific structures such as functionalized surfaces, particular hierarchical structures, and morphologies are preferred to deliver high electrochemical energy storage performance due to their efficient ion diffusion and charge storage capability. Meanwhile, active materials have low electrical conductivity or poor ion diffusion, which would result in low capacity under high current rate and limit their utilization. For instance, the intrinsic electrical conductivity of MoS₂ can be improved by V doping and rate performance of Li-ion battery was enhanced.^[151] Henceforth, by collecting the existing data (such as pure/doped material crystal structure, band structure, and its corresponding long cycle and rate performance) and creating appropriate descriptors, machine learning techniques could predict optimal battery material and accelerate DFT calculation optimization.

In addition, the volumetric performance based on the entire volume of devices is as important as gravimetric performance. The volumetric performance of electrochemical energy storage devices largely depends on electrode materials, binders, additives, current collectors, separators and electrolytes, and packaging. To design advanced electrode materials with high gravimetric and volumetric performances as well as a long cycle life, materials scientists propose various methods such as mechanical compression, capillary compression to densify materials.^[152] For example, the introduction of heavy and polar materials with suitable tap density is expected to achieve high electrode packing with high volumetric energy densities.^[153] Importantly, every single method is not independent and isolated, and future research should try to combine advantages and learn from each other to realize high-performance binder-free electrodes in the EES devices.

3.3. Electrode and Substrate Materials Selection and Structural Optimization

Currently, regardless of the binder-free electrode with a current collector or freestanding film, the power density, energy density and stability of the whole EES device should be enhanced before the commercialization of laboratory products. Among them, active materials as major factor in the electrochemistry performance should attract attention from researchers. For example, pseudo-capacitor materials quickly store charge through battery-like redox reactions, accomplishing high energy density at high power density.^[154] MXenes is one of the candidate materials that have a high surface area and a Faraday reaction, and is easy to insert ions between the 2D layers,^[154] which has the potential to be applied to a new generation of energy storage materials. Further research about the well-design structural can and address the “dead mass” problem to improve energy and power density. For instance, the embedding construction can shield adverse interactions and volume changes to enable transport structure stability of active particles. Simultaneously, the traditional untreated current collectors, e.g., copper or aluminum foil is more likely to form unstable and grow dendrites on the metal-electrolyte interface.^[155] Thus, further study is necessary whether there will be corresponding side reactions on the binder-free electrode substrate. Furthermore, the traditional collectors regularly play the role of supporting skeleton and electron conduction that is another “dead mass” for the binder-free electrode. To enrich their functions, the conductive and flexible matrix substrates such as carbon cloth and CNT thin films are candidates for flexible and wearable electronics. Due to prolonged contact with the human body, safety is the most important. Binder-free electrodes have high mechanical performance and stable electrochemical performance without toxic elements should be explored.

3.4. Trade-off between Energy Storage Performance and Commercialization

In general, these methods are still at the laboratory level and should be studied to provide more efficient production methods than traditional methods. Yao et al.^[156] reported that the carbothermal shock, that is a flash heating (~2000 K, shock duration of ~55 ms,) and cooling process, can apply multi-metallic nanoparticles uniformly dispersed on the carbon support. However, the electrochemistry performance of obtained materials remains to be investigated, and further research on the facile approaches for high-performance ESS electrode material should be investigated. Currently, the binder-free electrode tends to employ high-cost materials such as CF, rGO, and CNTs are commonly utilized as the framework for structural support, because of their lightweight, high electrical conductivity and outstanding electrochemical performance. While for large-scale application, it needs to consider to reduce the cost of substrates or find cheap alternatives. For active materials, researchers usually only premeditate excellent elec-

trochemistry performances but ignore cost. For industrial applications, a balance between energy storage performance and commercialization should be considered. Thus, further investigations for efficient, stable, low-cost, and environmentally friendly binder-free electrode for energy storage are required. Meanwhile, one important direction is to design a specific structure or develop suitable materials to guarantee ordered transport pathways and structural stability for a long life span.

Acknowledgements

This project was supported by National Key Research and Development Program of China (2019YFE0198000), Science and Technology Program of Guangzhou (2019050001), the Scientific and Technological Plan of Guangdong Province (2018A050506078, 2018B050502010), the Department of Education of Guangdong Province (2019KZDXM014, 2018KTSCX047), China Postdoctoral Science Foundation (2019 M662955), Natural Science Foundation of Guangdong Province (2019 A1515011615), SCNU Outstanding Young Scholar Project (8S0256), the Science and Technology Development Fund, Macau SAR (File no. 0191/2017/A3, 0041/2019/A1, 0046/2019/AFJ, 0021/2019/AIR), University of Macau (File no. MYRG2017-00216-FST and MYRG2018-00192-IAPME), and the UEA funding. F.C. acknowledges the Pearl River Talent Program (2019QN01 L951), and UEA Global Talent Research Fellowship.

Conflict of Interest

The authors declare that they have no known competing financial interests or personal relationships that could have appeared to influence the work reported in this paper.

Keywords: binder-free • freestanding electrode • batteries • supercapacitors • energy storage

- [1] B. Dunn, H. Kamath, J.-M. Tarascon, *Science* **2011**, *334*, 928–935.
- [2] Y. Zhou, X. Shao, K. H. Lam, Y. Zheng, L. Zhao, K. Wang, J. Zhao, F. Chen, X. Hou, *ACS Appl. Mater. Interfaces* **2020**, *12*, 30328–30335.
- [3] J. Ji, Y. Li, W. Peng, G. Zhang, F. Zhang, X. Fan, *Adv. Mater.* **2015**, *27*, 5264–5279.
- [4] W.-J. Song, S. Yoo, G. Song, S. Lee, M. Kong, J. Rim, U. Jeong, S. Park, *Batteries & Supercaps* **2019**, *2*, 181–199; *Supercaps* **2019**, *2*, 181–199.
- [5] J. Wang, Y. Cui, D. Wang, *Adv. Mater.* **2019**, *31*, 1801993.
- [6] S. Yun, Y. Zhang, Q. Xu, J. Liu, Y. Qin, *Nano Energy* **2019**, *60*, 600–619.
- [7] J. Chen, *Batteries & Supercaps* **2019**, *2*, 401–402; *Supercaps* **2019**, *2*, 401–402.
- [8] K. Shen, Z. Zhang, S. Wang, Q. Ru, L. Zhao, L. Sun, X. Hou, F. Chen, *Energy Fuels* **2020**, *34*, 8987–8992.
- [9] S. Yuan, X.-I. Huang, D.-I. Ma, H.-g. Wang, F.-z. Meng, X.-b. Zhang, *Adv. Mater.* **2014**, *26*, 2273–2279.
- [10] J. Guo, J. Liu, *Nanoscale Adv.* **2019**, *1*, 2104–2122.
- [11] H. Hosseini, S. Shahrokhian, *Chem. Eng. J.* **2018**, *341*, 10–26.
- [12] L. Li, W. Liu, F. Yang, W. Jiao, L. Hao, R. Wang, *Compos. Sci. Technol.* **2020**, *187*, 107946.
- [13] X. Xiong, W. Luo, X. Hu, C. Chen, L. Qie, D. Hou, Y. Huang, *Sci. Rep.* **2015**, *5*, 9254.
- [14] G. Q. Zhang, H. B. Wu, H. E. Hoster, M. B. Chan-Park, X. W. Lou, *Energy Environ. Sci.* **2012**, *5*, 9453–9456.
- [15] D. Sugumar, L. Kong, in *Encyclopedia of Microfluidics and Nanofluidics* (Ed.: D. Li), Springer New York, New York, NY, **2015**, pp. 422–429.
- [16] G. X. Wang, J.-h. Ahn, J. Yao, M. Lindsay, H. K. Liu, S. X. Dou, *J. Power Sources* **2003**, *119–121*, 16–23.
- [17] A. S. Arava Leela Mohana Reddy, S. R. Gowda, H. Gullapalli, M. Dubey, P. M. Ajayan, *ACS Nano* **2010**, *4*, 6337–6342.
- [18] S.-W. O. Indranil Lahiri, J. Y. Hwang, S. Cho, Y.-K. Sun, R. Banerjee, W. Choi, *ACS Nano* **2010**, *4*, 3440–3446.
- [19] in *Handbook of Deposition Technologies for Films and Coatings (Third Edition)* (Ed.: P. M. Martin), William Andrew Publishing, Boston, **2010**, pp. 1–31.
- [20] A. S. H. Makhlof, in *Nanocoatings and Ultra-Thin Films* (Eds.: A. S. H. Makhlof, I. Tiginyanu), Woodhead Publishing, **2011**, pp. 3–23.
- [21] S. Ullah, M. Hasan, H. Q. Ta, L. Zhao, Q. Shi, L. Fu, J. Choi, R. Yang, Z. Liu, M. H. Rümmeli, *Adv. Funct. Mater.* **2019**, *29*, 1904457.
- [22] Z. Cai, B. Liu, X. Zou, H.-M. Cheng, *Chem. Rev.* **2018**, *118*, 6091–6133.
- [23] H. Li, Y. Li, A. Aljarb, Y. Shi, L.-J. Li, *Chem. Rev.* **2018**, *118*, 6134–6150.
- [24] X. Wang, G. Yushin, *Energy Environ. Sci.* **2015**, *8*, 1889–1904.
- [25] X. Liu, L. Cao, Z. Guo, Y. Li, W. Gao, L. Zhou, *Materials* **2019**, *12*, 3304.
- [26] X. Ren, K. Turcheniuk, D. Lewis, W. Fu, A. Magasinski, M. W. Schauer, G. Yushin, *Small* **2018**, *14*, 1703425.
- [27] Z. Yao, L. Zhou, H. Yin, X. Wang, D. Xie, X. Xia, C. Gu, J. Tu, *Small* **2019**, *15*, 1904433.
- [28] N. C. Yeh, C. C. Hsu, J. Bagley, W. S. Tseng, *Nanotechnology* **2019**, *30*, 162001.
- [29] N. A. Maddock, N. L. James, D. R. McKenzie, J. F. Patrick, in *The Design and Manufacture of Medical Devices* (Eds.: J. Paulo Davim), Woodhead Publishing, **2012**, pp. 1–57.
- [30] M. Wuttke, Z. Liu, H. Lu, A. Narita, K. Müllen, *Batteries & Supercaps* **2019**, *2*, 929–933; *Supercaps* **2019**, *2*, 929–933.
- [31] Z. Bo, Y. Yang, J. Chen, K. Yu, J. Yan, K. Cen, *Nanoscale* **2013**, *5*, 5180–5204.
- [32] D. H. Seo, Z. J. Han, S. Kumar, K. K. Ostrikov, *Adv. Energy Mater.* **2013**, *3*, 1316–1323.
- [33] B. Ouyang, Y. Wang, Z. Zhang, R. S. Rawat, *Electrochim. Acta* **2016**, *194*, 151–160.
- [34] C. D. Wang, Y. S. Chui, Y. Li, X. F. Chen, W. J. Zhang, *Appl. Phys. Lett.* **2013**, *103*, 253903.
- [35] R. Paul, V. Etacheri, V. G. Pol, J. Hu, T. S. Fisher, *RSC Adv.* **2016**, *6*, 79734–79744.
- [36] Q. Zhang, Y. Wang, B. Zhang, K. Zhao, P. He, B. Huang, *Carbon* **2018**, *127*, 449–458.
- [37] Q. Zhang, N. Wei, P. Laiho, E. I. Kauppinen, *Top. Curr. Chem.* **2017**, *375*, 90.
- [38] E. X. Ding, H. Jiang, Q. Zhang, Y. Tian, P. Laiho, A. Hussain, Y. Liao, N. Wei, E. I. Kauppinen, *Nanoscale* **2017**, *9*, 17601–17609.
- [39] D. Song, W. Guo, T. Zhang, P. Lu, A. Guo, F. Hou, X. Yan, J. Liang, *Surface Innovations* **2019**, *7*, 10–17.
- [40] N. Mohammadian, S. M. Ghoreishi, S. Hafeziyeh, S. Saeidi, D. D. Dionysiou, *Nanomaterials* **2018**, *8*, 316.
- [41] A. Majeed, P.-X. Hou, S. Jiang, J.-C. Li, L.-Q. Ping, G.-X. Li, F. Zhang, C. Liu, H.-M. Cheng, *J. Mater. Chem. A* **2017**, *5*, 24813–24819.
- [42] Z. Wu, Z. Chen, X. Du, J. M. Logan, J. Sippel, M. Nikolou, K. Kamaras, J. R. Reynolds, D. B. Tanner, A. F. Hebard, A. G. Rinzler, *Science* **2004**, *305*, 1273–1276.
- [43] R. Karthick, F. Chen, *Carbon* **2019**, *150*, 292–310.
- [44] S. H. Ng, J. Wang, Z. P. Guo, J. Chen, G. X. Wang, H. K. Liu, *Electrochim. Acta* **2005**, *51*, 23–28.
- [45] S. H. N. Sua Yen Chew, J. Wang, P. Novaka, F. Krumeichc, S. Lei Choub, J. Chend, H. Kun Liu, *Carbon* **2009**, *47*, 2976–2983.
- [46] Z. Li, Y. Mi, X. Liu, S. Liu, S. Yang, J. Wang, *J. Mater. Chem.* **2011**, *21*, 14706.
- [47] G. Xu, C. Zheng, Q. Zhang, J. Huang, M. Zhao, J. Nie, X. Wang, F. Wei, *Nano Res.* **2011**, *4*, 870–881.
- [48] M. Q. Zhao, C. E. Ren, Z. Ling, M. R. Lukatskaya, C. Zhang, K. L. Van Aken, M. W. Barsoum, Y. Gogotsi, *Adv. Mater.* **2015**, *27*, 339–345.
- [49] P. Srimuk, J. Lee, S. Fleischmann, S. Choudhury, N. Jäckel, M. Zeiger, C. Kim, M. Aslan, V. Presser, *J. Mater. Chem. A* **2017**, *5*, 15640–15649.
- [50] B. Tang, L. Zhang, R. Li, J. Wu, M. N. Hedhili, P. Wang, *Nanoscale* **2016**, *8*, 1108–1116.
- [51] S. Zhao, M. Li, X. Wu, S. H. Yu, W. Zhang, J. Luo, J. Wang, Y. Geng, Q. Gou, K. Sun, *Mater. Today* **2020**, *6*, 100060.

- [52] G. Yuan, J. Xiang, H. Jin, Y. Jin, L. Wu, Y. Zhang, A. Mentbayeva, Z. Bakunov, *Electrochim. Acta* **2018**, *259*, 647–654.
- [53] Y. Kang, C. Deng, Y. Chen, X. Liu, Z. Liang, T. Li, Q. Hu, Y. Zhao, *Nanoscale Res. Lett.* **2020**, *15*, 112.
- [54] J. Cherusseri, D. Pandey, J. Thomas, *Batteries & Supercaps* **2020**, *3*, 860; *Supercaps* **2020**, *3*, 860.
- [55] X. Liu, X. Zhang, S. Ma, S. Tong, X. Han, H. Wang, *Electrochim. Acta* **2020**, *333*, 135568.
- [56] T. Chen, L. Dai, *Mater. Today* **2013**, *16*, 272–280.
- [57] H. Chen, L. Yu, Z. Lin, Q. Zhu, P. Zhang, N. Qiao, B. Xu, *J. Mater. Sci.* **2019**, *55*, 1148–1156.
- [58] S. Zhai, L. Wei, H. E. Karahan, Y. Wang, C. Wang, A. Montoya, Q. Shao, X. Wang, Y. Chen, *Carbon* **2018**, *132*, 698–708.
- [59] A. Rabenau, *Angew. Chem. Int. Ed. Engl.* **1985**, *24*, 1026–1040.
- [60] J. Zhao, Y. Tian, A. Liu, L. Song, Z. Zhao, *Mater. Sci. Semicond. Process.* **2019**, *96*, 78–90.
- [61] H. Zhong, T. Mirkovic, G. D. Scholes, in *Comprehensive Nanoscience and Technology* (Eds.: D. L. Andrews, G. D. Scholes, G. P. Wiederrecht), Academic Press, Amsterdam, **2011**, pp. 153–201.
- [62] B. G. Rao, D. Mukherjee, B. M. Reddy, in *Nanostructures for Novel Therapy* (Eds.: D. Ficai, A. M. Grumezescu), Elsevier, **2017**, pp. 1–36.
- [63] H. Li, Y.-J. Zhu, *Chem. Eur. J.* **2020**, *26*, 9180–9205.
- [64] P. Pazhamalai, K. Krishnamoorthy, S. Sahoo, V. K. Mariappan, S. J. Kim, *Chem. Eng. J.* **2019**, *359*, 409–418.
- [65] S. Yang, C. Wu, J. Cai, Y. Zhu, H. Zhang, Y. Lu, K. Zhang, *J. Mater. Chem. A* **2017**, *5*, 16776–16785.
- [66] Y. Liu, J. Sun, S. Lin, Z. Xu, L. Li, *J. Alloys Compd.* **2020**, *820*, 153113.
- [67] Y. Huang, S. Ge, X. Chen, Z. Xiang, X. Zhang, R. Zhang, Y. Cui, *Chemistry* **2019**, *25*, 14117–14122.
- [68] R. Zhang, X. Li, Y. Zhu, Y. Shen, A. Xie, *J. Alloys Compd.* **2019**, *810*, 151861.
- [69] Q. Li, H. Yao, F. Liu, Z. Gao, Y. Yang, *Electrochim. Acta* **2019**, *321*, 134682.
- [70] Y. Zhou, S. Zhao, X. Yu, Y. Li, H. Chen, L. Han, *Inorg. Chem. Front.* **2020**, *7*, 427–436.
- [71] G. Liu, C. Zhao, T. Liu, D. He, H. Suo, *Mater. Lett.* **2018**, *220*, 78–81.
- [72] H. Chen, L. Yu, J. M. Zhang, C. P. Liu, *Ceram. Int.* **2016**, *42*, 18058–18063.
- [73] Q. Xie, R. Song, P. Zhao, Y. Zhang, S. Wu, D. Xie, *J. Mater. Chem. A* **2018**, *6*, 8388–8395.
- [74] Y. Wang, Y. Xie, *J. Alloys Compd.* **2020**, *824*, 153936.
- [75] Z. Zhu, R. Zhang, J. Lin, K. Zhang, N. Li, C. Zhao, G. Chen, C. Zhao, *J. Power Sources* **2019**, *437*, 226941.
- [76] K. Cao, L. Jiao, Y. Liu, H. Liu, Y. Wang, H. Yuan, *Adv. Funct. Mater.* **2015**, *25*, 1082–1089.
- [77] Y. Liu, C. Zhang, X. Zhang, in *Recent Developments in the Field of Carbon Fibers*, **2018**.
- [78] J. Shen, X. Xu, J. Liu, Z. Liu, F. Li, R. Hu, J. Liu, X. Hou, Y. Feng, Y. Yu, M. Zhu, *ACS Nano* **2019**, *13*, 8986–8996.
- [79] B. Guo, S. Bandaru, C. Dai, H. Chen, Y. Zhang, Q. Xu, S. Bao, M. Chen, M. Xu, *ACS Appl. Mater. Interfaces* **2018**, *10*, 43707–43715.
- [80] T. Gao, C. Xu, R. Li, R. Zhang, B. Wang, X. Jiang, M. Hu, Y. Bando, D. Kong, P. Dai, X. B. Wang, *ACS Nano* **2019**, *13*, 11901–11911.
- [81] Q. Zhang, K. Zhou, J. Lei, W. Hu, *Appl. Surf. Sci.* **2019**, *467*, 992–999.
- [82] J. Kang, Q. Su, H. Feng, P. Huang, G. Du, B. Xu, *Electrochim. Acta* **2019**, *301*, 29–38.
- [83] Y. Zhang, H. Tao, T. Li, S. Du, J. Li, Y. Zhang, X. Yang, *ACS Appl. Mater. Interfaces* **2018**, *10*, 35206–35215.
- [84] M. Ramu, J. R. Chellan, N. Goli, P. Joaquim, V. Cristobal, B. C. Kim, *Adv. Funct. Mater.* **2019**, *30*, 1906586.
- [85] X. Xu, X. Tian, X. Li, T. Yang, Y. He, K. Wang, Y. Song, Z. Liu, *Appl. Surf. Sci.* **2019**, *465*, 635–642.
- [86] F. Ma, X. Dai, J. Jin, N. Tie, Y. Dai, *Electrochim. Acta* **2020**, *331*, 135459.
- [87] Y. Yue, H. Liang, *Adv. Energy Mater.* **2017**, *7*, 1602545.
- [88] J. Yao, Y. Li, R. C. Massé, E. Uchaker, G. Cao, *Energy Storage Mater.* **2018**, *11*, 205–259.
- [89] D. Kong, X. Li, Y. Zhang, X. Hai, B. Wang, X. Qiu, Q. Song, Q.-H. Yang, L. Zhi, *Energy Environ. Sci.* **2016**, *9*, 906–911.
- [90] J. M. Son, S. Oh, S. H. Bae, S. Nam, I. K. Oh, *Adv. Energy Mater.* **2019**, *9*, 1900477.
- [91] H. Chen, J. He, G. Ke, L. Sun, J. Chen, Y. Li, X. Ren, L. Deng, P. Zhang, *Nanoscale* **2019**, *11*, 16253–16261.
- [92] B. Cai, A. Eychmuller, *Adv. Mater.* **2019**, *31*, 1804881.
- [93] G. Gorgolis, C. Galiotis, *2D Mater.* **2017**, *4*, 032001.
- [94] H. Chu, Y. Pei, Z. Cui, C. Steven, P. Dong, P. M. Ajayan, M. Ye, J. Shen, *Nanoscale* **2018**, *10*, 14697–14704.
- [95] S. M. Jung, H. Y. Jung, M. S. Dresselhaus, Y. J. Jung, J. Kong, *Sci. Rep.* **2012**, *2*, 849.
- [96] D. W. Kim, S. M. Jung, H. Y. Jung, *J. Mater. Chem. A* **2020**, *8*, 532–542.
- [97] B. Yao, S. Chandrasekaran, H. Zhang, A. Ma, J. Kang, L. Zhang, X. Lu, F. Qian, C. Zhu, E. B. Duoss, C. M. Spadaccini, M. A. Worsley, Y. Li, *Adv. Mater.* **2020**, *32*, e1906652.
- [98] C. H. A. Tsang, H. Huang, J. Xuan, H. Wang, D. Y. C. Leung, *Renewable Sustainable Energy Rev.* **2020**, *120*, 109656.
- [99] L. Wang, G. Yang, S. Peng, J. Wang, W. Yan, S. Ramakrishna, *Energy Storage Mater.* **2020**, *25*, 443–476.
- [100] Q. Liu, J. Zhu, L. Zhang, Y. Qiu, *Renewable Sustainable Energy Rev.* **2018**, *81*, 1825–1858.
- [101] E. S. Pampal, E. Stojanovska, B. Simon, A. Kilic, *J. Power Sources* **2015**, *300*, 199–215.
- [102] K. Shen, H. Chen, X. Hou, S. Wang, H. Qin, Y. Gao, J. Shen, *Ionics* **2020**, *26*, 3297–3305.
- [103] A. S. Levitt, M. Alhabeb, C. B. Hatter, A. Sarycheva, G. Dion, Y. Gogotsi, *J. Mater. Chem. A* **2019**, *7*, 269–277.
- [104] Y. Zheng, in *Bioinspired Design of Materials Surfaces* (Ed.: Y. Zheng), Elsevier, **2019**, pp. 99–146.
- [105] P. Vass, E. Szabo, A. Domokos, E. Hirsch, D. Galata, B. Farkas, B. Demuth, S. K. Andersen, T. Vigh, G. Verreck, G. Marosi, Z. K. Nagy, *WIRE Nanomed. Nanobiotechnol.* **2019**, *12*, e1611.
- [106] W. Li, R. Fang, Y. Xia, W. Zhang, X. Wang, X. Xia, J. Tu, *Batteries & Supercaps* **2019**, *2*, 9–36; *Supercaps* **2019**, *2*, 9–36.
- [107] R. Jose Varghese, E. h M Sakho, S. Parani, S. Thomas, O. S. Oluwafemi, J. Wu, in *Nanomaterials for Solar Cell Applications* (Eds.: S. Thomas, E. H. M. Sakho, N. Kalarikkal, S. O. Oluwafemi, J. Wu), Elsevier, **2019**, pp. 75–95.
- [108] R. Chen, Y. Hu, Z. Shen, P. Pan, X. He, K. Wu, X. Zhang, Z. Cheng, *J. Mater. Chem. A* **2017**, *5*, 12914–12921.
- [109] S. Yao, S. Xue, S. Peng, M. Jing, X. Shen, T. Li, Z. YiLiu, *Int. J. Energy Res.* **2019**, *43*, 1892–1902.
- [110] F. Wang, N. Zhang, X. Zhao, L. Wang, J. Zhang, T. Wang, F. Liu, Y. Liu, L. Z. Fan, *Adv. Sci.* **2019**, *6*, 1900649.
- [111] Z. Chen, H. Duan, Z. Xu, C. Chen, Y. Yan, S. Wu, *Adv. Mater. Interfaces* **2020**, *7*, 1901922.
- [112] B. Zhang, F. Kang, J.-M. Tarascon, J.-K. Kim, *Prog. Mater. Sci.* **2016**, *76*, 319–380.
- [113] C. Wang, Y. V. Kaneti, Y. Bando, J. Lin, C. Liu, J. Li, Y. Yamauchi, *Mater. Horiz.* **2018**, *5*, 394–407.
- [114] G. Yang, L. Wang, J. Wang, W. Yan, *Mater. Lett.* **2016**, *177*, 13–16.
- [115] X. Huang, J. Liu, Z. Huang, X. Ke, L. Liu, N. Wang, J. Liu, Z. Guo, Y. Yang, Z. Shi, *Electrochim. Acta* **2020**, *333*, 135493.
- [116] U. Gunputh, H. Le, in *Biomedical Composites (Second Edition)* (Ed.: L. Ambrosio), Woodhead Publishing, **2017**, pp. 111–138.
- [117] L. Oakes, A. Westover, M. Mahjouri-Samani, S. Chatterjee, A. A. Puretzky, C. Rouleau, D. B. Geohegan, C. L. Pint, *ACS Appl. Mater. Interfaces* **2013**, *5*, 13153–13160.
- [118] S. Obregon, G. Amor, A. Vazquez, *Adv. Colloid Interface Sci.* **2019**, *269*, 236–255.
- [119] S. Heise, L. Ramos Rivera, A. R. Boccaccini, in *Biomedical, Therapeutic and Clinical Applications of Bioactive Glasses* (Ed.: G. Kaur), Woodhead Publishing, **2019**, pp. 3–33.
- [120] R. Garg, S. Elmas, T. Nann, M. R. Andersson, *Adv. Energy Mater.* **2017**, *7*, 1601393.
- [121] A. R. Boccaccini, J. Cho, J. A. Roether, B. J. C. Thomas, E. Jane Minay, M. S. P. Shaffer, *Carbon* **2006**, *44*, 3149–3160.
- [122] M. Li, N. Muralidharan, K. Moyer, C. L. Pint, *Nanoscale* **2018**, *10*, 10443–10449.
- [123] L. Li, W. Liu, F. Yang, W. Jiao, L. Hao, R. Wang, *Compos. Sci. Technol.* **2020**, *187*, 107946.
- [124] J. Cherusseri, K. Sambath Kumar, D. Pandey, E. Barrios, J. Thomas, *Small* **2019**, *15*, 1902606.
- [125] C. Augello, H. Liu, in *Surface Modification of Magnesium and its Alloys for Biomedical Applications* (Eds.: T. S. N. S. Narayanan, I.-S. Park, M.-H. Lee), Woodhead Publishing, **2015**, pp. 335–353.
- [126] S. Arulmani, S. Anandan, M. Ashokkumar, in *Nanomaterials for Green Energy* (Eds.: B. A. Bhanvase, V. B. Pawade, S. J. Dhoble, S. H. Sonawane, M. Ashokkumar), Elsevier, **2018**, pp. 1–53.
- [127] G. Nagaraju, Y. H. Ko, S. M. Cha, S. H. Im, J. S. Yu, *Nano Res.* **2016**, *9*, 1507–1522.
- [128] S. C. Sekhar, G. Nagaraju, J. S. Yu, *Nano Energy* **2017**, *36*, 58–67.

- [129] N. Zhang, M. Jia, Y. Dong, Y. Wang, J. Xu, Y. Liu, L. Jiao, F. Cheng, *Adv. Funct. Mater.* **2019**, *29*, 1807331.
- [130] J. Xue, T. Wu, Y. Dai, Y. Xia, *Chem. Rev.* **2019**, *119*, 5298–5415.
- [131] S. Ramakrishna, R. Jose, P. S. Archana, A. S. Nair, R. Balamurugan, J. Venugopal, W. E. Teo, *J. Mater. Sci.* **2010**, *45*, 6283–6312.
- [132] P. Amrollahi, J. S. Krasinski, R. Vaidyanathan, L. Tayebi, D. Vashaee, in *Handbook of Nanoelectrochemistry: Electrochemical Synthesis Methods, Properties, and Characterization Techniques* (Eds.: M. Aliofkhazraei, A. S. H. Makhlof), Springer International Publishing, Cham, **2016**, pp. 561–591.
- [133] L. Liang, Y. Xu, Y. Li, H. Dong, M. Zhou, H. Zhao, U. Kaiser, Y. Lei, *J. Mater. Chem. A* **2017**, *5*, 1749–1755.
- [134] G. Thandapani, E. Radha, J. Jayashri, J. Annie Kamala Florence, P. N. Sudha, in *Fundamental Biomaterials: Metals* (Eds.: P. Balakrishnan, S. M. S. Thomas), Woodhead Publishing, **2018**, pp. 79–110.
- [135] B. Yao, J. Zhang, T. Kou, Y. Song, T. Liu, Y. Li, *Adv. Sci.* **2017**, *4*, 1700107.
- [136] J. Wang, B. Liu, *Sci. Technol. Adv. Mater.* **2019**, *20*, 992–1009.
- [137] J.-H. Lee, S.-J. Park, *Carbon* **2020**, *163*, 1–18.
- [138] J. Huo, Y. Xue, L. Zhang, X. Wang, Y. Cheng, S. Guo, *J. Colloid Interface Sci.* **2019**, *555*, 791–800.
- [139] J. Guan, Y. Chen, L. Cao, Y. Liu, P. Lian, Y. Gao, X. Shi, *J. Power Sources* **2020**, *469*, 228307.
- [140] L. Xue, S. V. Savilov, V. V. Lunin, H. Xia, *Adv. Funct. Mater.* **2018**, *28*, 1705836.
- [141] Y. Huang, A. Buffa, H. Deng, S. Sarkar, Y. Ouyang, X. Jiao, Q. Hao, D. Mandler, *J. Power Sources* **2019**, *439*, 227046.
- [142] A. I. Inamdar, H. S. Chavan, A. T. Aqueel Ahmed, Y. Jo, S. Cho, J. Kim, S. M. Pawar, H. Kim, H. Im, *J. Alloys Compd.* **2020**, *829*, 154593.
- [143] P. C. Ghimire, R. Schweiss, G. G. Scherer, N. Wai, T. M. Lim, A. Bhattacharai, T. D. Nguyen, Q. Yan, *J. Mater. Chem. A* **2018**, *6*, 6625–6632.
- [144] Y.-S. Liu, C. Ma, Y.-L. Bai, X.-Y. Wu, Q.-C. Zhu, X. Liu, X.-H. Liang, X. Wei, K.-X. Wang, J.-S. Chen, *J. Mater. Chem. A* **2018**, *6*, 17473–17480.
- [145] A. Levitt, J. Zhang, G. Dion, Y. Gogotsi, J. M. Razal, *Adv. Funct. Mater.* **2020**, *30*, 2000739.
- [146] H. Li, X. Zhang, Z. Zhao, Z. Hu, X. Liu, G. Yu, *Energy Storage Mater.* **2020**, *26*, 83–104.
- [147] J. Hong, W. E. Gent, P. Xiao, K. Lim, D.-H. Seo, J. Wu, P. M. Csernica, C. J. Takacs, D. Nordlund, C.-J. Sun, K. H. Stone, D. Passarelli, W. Yang, D. Prendergast, G. Ceder, M. F. Toney, W. C. Chueh, *Nat. Mater.* **2019**, *18*, 256–265.
- [148] Y. Zhou, W. Shan, X. Hou, K.-h. Lam, X. Zhao, X. Liu, Y. Wu, *Solid State Ionics* **2020**, *350*, 115326.
- [149] O. Borodin, *Curr. Opin. Electrochem.* **2019**, *13*, 86–93.
- [150] S. Choudhury, Z. Tu, A. Nijamudheen, M. J. Zachman, S. Stalin, Y. Deng, Q. Zhao, D. Vu, L. F. Kourkoutis, J. L. Mendoza-Cortes, L. A. Archer, *Nat. Commun.* **2019**, *10*, 3091.
- [151] Y. Lei, K. Fujisawa, F. Zhang, N. Briggs, A. R. Aref, Y.-T. Yeh, Z. Lin, J. A. Robinson, R. Rajagopalan, M. Terrones, *ACS Appl. Mater. Interfaces* **2019**, *2*, 8625–8632.
- [152] Q. Wang, J. Yan, Z. Fan, *Energy Environ. Sci.* **2016**, *9*, 729–762.
- [153] T. Wu, J. Qi, M. Xu, D. Zhou, Z. Xiao, *ACS Nano* **2020**, *14*, 15011–15022.
- [154] C. Choi, D. S. Ashby, D. M. Butts, R. H. DeBlock, Q. Wei, J. Lau, B. Dunn, *Nat. Rev. Mater.* **2020**, *5*, 5–19.
- [155] W. Liu, P. Liu, D. Mitlin, *Chem. Soc. Rev.* **2020**, *49*, 7284–7300.
- [156] Y. Yao, Z. Huang, P. Xie, S. D. Lacey, R. J. Jacob, H. Xie, F. Chen, A. Nie, T. Pu, M. Rehwoldt, D. Yu, M. R. Zachariah, C. Wang, R. Shahbazian-Yassar, J. Li, L. Hu, *Science* **2018**, *359*, 1489–1494.

Manuscript received: November 9, 2020

Revised manuscript received: December 29, 2020

Accepted manuscript online: December 30, 2020

Version of record online: February 2, 2021